W7-AS Contributions to the 7th Toki Conference,
28 November - 1 December 1995,
Toki City, Japan

IPPIII/210 März 1996

MAX-PLANCK-INSTITUT FÜR PLASMAPHYSIK

85748 GARCHING BEI MÜNCHEN

MAX-PLANCK-INSTITUT FÜR PLASMAPHYSIK

GARCHING BEI MÜNCHEN

W7-AS Contributions to the 7th Toki Conference,
28 November - 1 December 1995,
Toki City, Japan

IPP III 210 März 1996

Die nachstehende Arbeit wurde im Rahmen des Vertrages zwischen dem Max-Planck-Institut für Plasmaphysik und der Europäischen Atomgemeinschaft über die Zusammenarbeit auf dem Gebiete der Plasmaphysik durchgeführt.

W7-AS Contributions to the7th Toki Conference

28 November - 1 December 1995,

Toki City, Japan

CONTENTS

TEMPERATURE FLUCTUATION MEASUREMENTS WITH ECE AT W7-AS

H.J. Hartfuss, S. Sattler, M. Häse, M. Hirsch, T. Geist, W7-AS Team

Max-Planck-Institut für Plasmaphysik, EURATOM-Ass., 85748 Garching, Germany

Abstract

The diagnostic difficulties in measuring electron temperature fluctuations with a relative level below 1% are outlined. It is shown that correlation radiometry of electron cyclotron emission provides sufficient sensitivity to overcome the limit set by intensity fluctuations of thermal radiation. The experimental set-up used for the first measurements is described as well as the first results obtained at the W7-AS stellarator. With an extended arrangement a first comparison between the two different correlation schemes as developed at W7-AS and at TEXT became possible.

1. Introduction

A significant amount of the anomalously high electron heat transport is assumed to be driven by fluctuations of density, electric field, temperature, and magnetic field excited by plasma instabilities. Independent of the driving mechanisms the electrostatic term of the temperature fluctuation driven heat flux is given by $\tilde{q}_e \propto n_e \langle \tilde{E}_\Theta \tilde{T}_e \rangle$ where n_e is the local electron density and $\tilde{E}_\Theta$ the fluctuating poloidal electric field (Liewer [1], Wootton et al. [2]). Temperature fluctuations have been measured at the plasma edge with probes (Hidalgo et al. [3], Giannone et al. [4]). In the confinement region they have been shown to exist applying the correlation method described below (Sattler and Hartfuss [5]). The search for fluctuations was governed by properties of density fluctuation as

known from coherent microwave or laser scattering, i.e. wave vectors < 10 cm^{-1} and frequencies < 1 MHz. Hence the fluctuation sensitive diagnostic has to have temporal and spatial resolution in the 10^{-6} s and 10^{-2} m ranges. High sensitivity to small fluctuation amplitudes is required since relative amplitudes below 1% might significantly contribute to transport. Due to the fact that none of the existing core temperature diagnostics fulfills these requirements new approaches had to be found. The purpose of this paper is to describe in some detail the diagnostic problem and the techniques applied to detect turbulent temperature fluctuations in the core of a magnetically confined plasma for the first time. Two methods both based on correlation radiometry of electron cyclotron emission (ECE) have successfully been applied, the crossed sightline technique as developed at W7-AS (Sattler and Hartfuss [5]), and the correlation of ECE channels overlapping in real space but separated in frequency space as developed at TEXT (Kwon [6], Cima [14]). For a comparison of the methods the crossed sightline set-up at W7-AS has been supplemented in such a way that the application of the second method is simultaneously possible. First results are being discussed. In the context of temperature fluctuation measurements the density fluctuations present in the observed plasma volume play an important role. An experimental arrangement as built up at W7-AS is presented which is dedicated to the question whether temperature and density fluctuations are correlated. Search for it has been started. Details of the temperature fluctuation behaviour although provided by this method are not the subject of this paper but first parameter scans conducted at W7-AS are included.

2. Diagnostic Problem

Measurement of the electron temperature in the plasma core by heterodyne radiometry of an optically thick harmonic of the ECE has the potential of sufficient spatial and temporal resolution but the required sensitivity for small fluctuation amplitudes is limited by natural fluctuations of the ECE due to the thermal nature of the radiation. The electrons contributing to the ECE of an optically thick mode can be assumed to be in local thermodynamic equilibrium. The intensity of the ECE then reaches the blackbody level and the measured radiation temperature approaches the electron temperature. The ECE spectrum observed is determined by the local temperature and the B-field excursion along the line of sight. Although it differs significantly from the spectrum of a blackbody source, the ECE can be treated as linearly filtered blackbody radiation. In this case the statistical properties of the radiation field remain conserved (Mandel and Wolf [7], Davenport and Root [8]). The coherence properties of thermal radiation are therefore applicable to electron cyclotron emission, too.

To determine the natural fluctuations of thermal radiation, a purely classical description can be used because of the high average photon occupation number $\langle n \rangle$ of the order of 10^6 in case of a cavity mode in thermal equilibrium (500 eV, 140 GHz). Then the photon and the classical wave pictures are equivalent. In the frame of the cavity mode description the natural fluctuations of the radiation are fluctuations Δn of the occupation number, the mean square of the fluctuations are given by $\langle \Delta n^2 \rangle = \langle n \rangle^2 + \langle n \rangle$. The first term can be attributed to the wave character, the second term -completely negligible in the classical case $n >> 1$ under consideration- to the particle nature of light, Loudon [9].

Assuming the intensity I(t) of a thermal source of constant temperature to be composed of a time averaged constant part <I(t)> and a fluctuating part i(t), I(t) = <I(t)> + i(t), the crosscorrelation function of the fluctuating parts $i_1(t)$ and $i_2(t)$ measured at two points P_1 and P_2 in space is given by:

$$\langle i_1(t)\, i_2(t)\rangle = \langle I_1(t) I_2(t)\rangle - \langle I_1(t)\rangle\langle I_2(t)\rangle = \left|\gamma_{12}(0)\right|^2 \langle I_1(t)\rangle\langle I_2(t)\rangle. \qquad (1)$$

Here the second order correlation function, $\langle I_1(t) I_2(t)\rangle$, has been expressed by the correlation of the corresponding electric fields E_1 and E_2, Loudon [9], by introducing the normalized coherence function, $\left|\gamma_{12}(\tau)\right|^2 = \left\langle E_1(t) E_2^*(t+\tau)\right\rangle \left(\langle I_1(t)\rangle\langle I_2(t)\rangle\right)^{-1/2}$.

Equation (1) links coherence (through γ_{12}) and intensity fluctuations (through $i_1 i_2$) of a thermal light source. It is the basis of the intensity interferometry as introduced by Hanbury-Brown and Twiss [10]. The crossed sightline correlation experiment as built up at W7-AS makes use of this relation to decorrelate the thermal fluctuations in an experimental arrangement with $\gamma_{12}(0) = 0$.

If the locations P_1 and P_2 coincide, resulting in $\gamma_{12} = 1$ by definition, the thermal noise in a detection system can be determined. In this case, $\left\langle i(t)^2\right\rangle = \left\langle I(t)\right\rangle^2$, which is the classical analogon to $\left\langle \Delta n^2\right\rangle = \langle n\rangle^2$. This result holds for an ideal detector with a response time τ_i much shorter than the coherence time τ_r of the radiation. If τ_i is larger than τ_r, the correlation is reduced by the factor τ_r / τ_i.

Applying heterodyne radiometry to detect thermal radiation, τ_r^{-1} is determined by the predetection bandwidth B_{if}, while τ_i^{-1} is determined by twice the postdetection bandwidth $2B_v$. The relative fluctuation level in measurements with a single detector is then given by an expression equivalent to the radiometer formula:

$$\frac{\sqrt{\langle i(t)^2 \rangle}}{\langle I(t) \rangle} = \sqrt{\frac{2B_v}{B_{if}}} \qquad (2)$$

This is the minimum level possible. It does not include the noise produced by the detector itself which is usually negligible in measurements at high temperature plasmas. If incoherent detection systems are used which are sensitive to a number of modes m, the relative fluctuation level is reduced by $1/\sqrt{m}$ (Storey [11], Hartfuss [12]).

The relations discussed so far hold for constant temperature of the blackbody emitter, or, in case a magnetized plasma is viewed, for constant electron temperature of the emitting layer. In ECE radiometry B_v determines the temporal resolution of the diagnostic and B_{if} determines its spatial resolution. To fulfill the demands for fluctuation measurements, B_v and B_{if} are typically 1 MHz and 500 MHz respectively, resulting in about 6% fluctuation level. If true temperature fluctuations are expected to occur with a relative level of less than 1%, they will completely be buried in the fluctuations of the thermal radiation which is called thermal noise in the following.

Considering now temperature fluctuations of the radiation source, the fluctuating part i(t) of the intensity is then composed of the temperature fluctuations $\tilde{T}(t)$ and the thermal noise n(t), $i(t) = \tilde{T}(t) + n(t)$. If the two contributions are statistically independent, $\langle \tilde{T}(t)\, n(t) \rangle = 0$, the correlation of the fluctuating parts $i_1(t)$ and $i_2(t)$ as emitted from positions r_1 and r_2 and measured by two detectors, can be written in the form

$$\begin{aligned} \langle i_1(t) i_2(t+\tau) \rangle &= \langle \tilde{T}_1(t) \tilde{T}_2(t+\tau) \rangle + \langle n_1(t) n_2(t+\tau) \rangle \\ &= \gamma_{\tilde{T}}(r_1, r_2, \tau) \sqrt{\langle \tilde{T}_1^2(t) \rangle \langle \tilde{T}_2^2(t) \rangle} + \gamma_n(r_1, r_2, \tau, \Theta) \sqrt{\langle n_1^2(t) \rangle \langle n_2^2(t) \rangle} \end{aligned} \qquad (3)$$

where the functions $\gamma_{\tilde{T}}$ and γ_n are the normalized crosscorrelations of the temperature fluctuations and the thermal noise respectively,

$$\gamma_{\tilde{T}}(r_1, r_2, \tau) = \frac{\left\langle \tilde{T}_1(t)\tilde{T}_2(t+\tau)\right\rangle}{\sqrt{\left\langle \tilde{T}_1^2(t)\right\rangle\left\langle \tilde{T}_2^2(t)\right\rangle}}, \quad \gamma_n(r_1, r_2, \tau, \Theta) = \frac{\left\langle n_1(t)n_2(t+\tau)\right\rangle}{\sqrt{\left\langle n_1^2(t)\right\rangle\left\langle n_2^2(t)\right\rangle}} \tag{4}$$

If experimental situations can be realized with $\gamma_{\tilde{T}} = 1$ and $\gamma_n = 0$, cross correlation techniques can be applied to overcome the sensitivity limit set by thermal noise.

(i) At W7-AS a common plasma volume is observed with two radiometers viewing along two different lines of sight. In this case $r_1 = r_2$ and the maximum of $\gamma_{\tilde{T}}$ occurs at $\tau = 0$ resulting in $\gamma_{\tilde{T}} = 1$. As a consequence of the coherence properties of thermal radiation, γ_n depends on the distance of the two detectors which can be transformed into the angle Θ enclosed by the two sightlines. If Θ exceeds a minimum value Θ_d, the thermal noise is completely uncorrelated resulting in $\gamma_n = 0$. The maximum of the cross correlation function then gives the rms fluctuation level of the temperature fluctuations, the quantity of interest, $\langle i_1(t)i_2(t+\tau)\rangle = \left\langle \tilde{T}_1^2(t)\right\rangle$. The calculation of the decorrelation angle Θ_d can be found in Sattler [13] and Sattler and Hartfuss [14]. It turns out to be 4^o at the crossed sightline experiment of W7-AS.

(ii) The second method as developed at TEXT makes use of the fact that in ECE measurements each frequency component is composed of emissions from slightly separated nearby radial locations, or, vice versa, that slightly different frequencies correspond to an overlapping radial range (Kwon [6], Cima [14]. Due to the fact that different spectral components are incoherent by definition, the correlation of two ECE

channels of a single sightline with slightly different frequencies results in $\gamma_n = 0$ with $r_1 \approx r_2$ and $\gamma_{\tilde{T}} \approx 1$.

3. Experimental Approach

The crossed sightline intensity interferometer arrangement of W7-AS consists in its basic version of two identical 4 channel heterodyne radiometers of the multichannel single sideband type (Hartfuss and Tutter [15]). They are absolutely calibrated and are designed to measure the second harmonic X-mode radiation around 145 GHz corresponding to the gradient region of the high field side of the electron temperature profile (at $B_0 = 2.5$ T), covering the radial range $0.53 < r / a_{separatrix} < 0.75$. The high field side has been chosen to avoid interference with relativistically down shifted emission of suprathermal electrons contributing to the low field side ECE. The sightlines enclosing an angle of about 20 degrees are defined by means of adjustable Gaussian beam optics. Elliptical mirrors in connection with corrugated horns are installed inside the vacuum vessel forming a slim beam with a waist of less than 20 mm. The two radiometers (whose mixers in the frontend share a common local oscillator) are well shielded from each other to avoid any electronic crosstalk. The filters in the intermediate frequency part have a bandwidth of 500 MHz which means the radial resolution is less than 1 cm. The filters are separated by about 1 GHz. The video bandwidth defining the temporal resolution is 1 MHz. With the aid of a specially developed quasithermal microwave source extensive laboratory tests have been conducted to test the properties of the correlation radiometers and to determine the decorrelation angle (Sattler and Hartfuss [13]). The sensitivity of the intensity interferometer to temperature fluctuations

is limited by the statistical error in the correlation function. It is determined by the number of samples used for calculating the correlation function and by the bandwidth ratio of Eq.(2). With 4 10^6 points the minimum detectable relative temperature fluctuation level is lower than 0.2%. Long stationary phases of the plasma discharges are necessary to reach this sensitivity level. The method has therefore no time resolution. The resolution in k-space which is important for the interpretation of the fluctuation levels and spectra, is given by the characteristics of the Gaussian beams and the radial resolution. Only fluctuating structures larger than the dimensions of the beam can be detected. This means that an integration of the k-spectrum takes place. In magnetic coordinates the k-spectrum is integrated down to $k_r = 1.4\ cm^{-1}$ in radial direction and down to $k_\perp = 2.3\ cm^{-1}$ transverse to the beam. With the system as described so far evidence for the existence of temperature fluctuations in W7-AS has been found. The results are briefly summarized in the next chapter.

4. Results

Results of temperature fluctuation measurements obtained with the 4 channel crossed sightline set-up are described in Sattler and Hartfuss [5], [16]. They are only briefly repeated here. Purely ECRH heated plasmas characterized by a central electron temperature and density of 1.3 keV and 4 10^{19} m^{-3} respectively are diagnosed. Three well distinguishable fluctuation phenomena have been found: turbulent fluctuations in the spectral ranges < 15 kHz and < 150 kHz and coherent modes in the 10 kHz range. Fig.1 gives the spectra measured. The fluctuation level of the turbulent components increases in the range 0.5 < r/a < 0.75 from 0.3% to about 1% in case of the low

frequency component and from 0.3% to 0.6 % for the high frequency one. The two turbulent components can also be distinguished by their different behaviour concerning radial and poloidal correlations. The crossed sightline arrangement allows to separate the emission volumes by tilting the two elliptical mirrors. Although no absolute measurement of the fluctuation level is possible with this adjustment, it allows measurements of poloidal motions. Poloidal velocities close to the electron diamagnetic drift velocity are found for the high frequency component while no poloidal velocity is found below 15 kHz. The signals in the 4 radial channels of each sightline provide information on radial correlations. The maximum of the cross correlation function is shifted in time providing a radial velocity of about 50 m/s directed from the plasma center to the edge. In addition a phase shift of π (anti-correlation) is observed after a radial distance of Δr = 2.3 cm. The high frequency fluctuations do not show a significant shift in time, however they decorrelate after a radial distance Δr = 2 cm, no anti-correlation is observed. The radial velocity of the low frequency fluctuations depends on the magnetic configuration of W7-AS as defined by the edge value of the rotational transform ι. It seems that for specific values of ι the radial velocity is zero.

First parameter scans have been conducted to determine the parameter dependence of temperature fluctuations on heating power and electron density (cf. Figs.2a and 2b). In the power scan the fluctuation level decreases whereas the confinement deteriorates. The expected correlation, increasing fluctuation level with decreasing confinement, has not been observed. In the density scan below about 4 10^{19} m^{-3} the fluctuation level

decreases with increasing density. Simultaneously the confinement improves. Above this value electron diffusivity saturates while the fluctuation level increases.

The results may indicate that the observed temperature fluctuation levels do not affect confinement at all or that the transport relevance of temperature fluctuations can increase though the amplitude decreases. Nothing is known about poloidal E-field fluctuations necessary to drive a radial heat flux.

5. Comparison with other Techniques

For simultaneous measurements with the two different correlation methods described, the bandfilters in the crossed sightline radiometers have recently been exchanged with those of 150 MHz bandwidth. In one of the radiometers additional 8 filters are installed. The 12 filters have a frequency separation of 300 MHz without overlap. The radiometer frontend and the observation geometry are unchanged.

Fig.3 gives for a typical experimental situation (T_{e0} = 1.7 keV, n_{e0} = 3 10^{19} m^{-3}) the emissivity as expressed by

$$G(R) = T_e(R)\,\alpha(R)\,e^{-\eta(R)}, \quad \eta(R) = \int_R^{ant} \alpha(R')dR' \qquad (5)$$

for two channels neighbouring in frequency space as a function of the coordinate R along the line of sight. The FWHM of the emission profiles is typically 3 mm. Neighbouring channels overlap in real space. Crosscorrelations are calculated for equivalent channels of the crossed sightline arrangement as well as for successive neighbouring channels. Low and high frequency components of the turbulent spectrum are evaluated separately. Fig.4 gives the results. The fluctuation amplitudes measured with the two different methods fit well together. Though, both techniques reveal their

distinct differences looking at the time shifts of the crosscorrelation maximum. Correlating neighboured channels, perfectly overlapping emission volumes are impossible. Any radial velocity of fluctuations therefore causes the signal to appear with a certain delay in different radial channels. This time shift clearly seen in Fig.4b is corresponding to a radial velocity of about 90 m/s. The crossed sightlines technique has in this respect a somewhat higher flexibility. Perfect overlap of the emission volumes in addition with completely separated radiometers and sightlines avoiding any correlated crosstalk, basically important for the proof of principle experiment, provides an instrumentation able to measure radial as well as poloidal correlation.

6. Error Discussion and Future Work

A number of systematic errors can influence the results. The most importants are cross talk from fluctuations of other physical parameters causing fluctuations of the radiation temperature. Three different effects, B-field fluctuations, plasma diamagnetism and variation of the depth of the emitting layer, can vary the location of the emission volume resulting in apparent temperature fluctuations in the presence of a temperature gradient. All these effects turn out to be negligible or at least small compared to the modulation from density fluctuations under finite optical depth conditions (Sattler [13]).

Due to the proportionality of the optical depth to the product of density and temperature, $\eta \propto n_e T_e$, radiation temperature fluctuations are caused by fluctuations of density and electron temperature, $\frac{\tilde{T}_R}{T_R} = (1+a)\frac{\tilde{T}_e}{T_e} + a\frac{\tilde{n}_e}{n_e}$, $a = \frac{\langle\eta\rangle e^{-\langle\eta\rangle}}{1-e^{-\langle\eta\rangle}}$.

Unfortunately the density fluctuations are not known with sufficent accuracy. In order to overcome this uncertainty, temperature and density fluctuations have to be measured simultaneously in the same plasma volume. A combination of ECE crossed sightline radiometers and a reflectometer are installed at W7-AS for this kind of measurement. Both diagnostics share the same pair of corrugated horn antennas and elliptical mirrors for Gaussian beam optics, specially designed to operate both in the microwave D-band around 140 GHz for the ECE measurements and in the W-band between 75 and 105 GHz for X-mode reflectometer measurements (Fig.5). The crossed sightline intensity interferometer uses 2 times 10 channels to cover the radial range accessible with the reflectometer. Search for temperature-density correlations has been started by scanning the reflectometer frequency on a shot-to-shot basis. The very large amount of data obtained at sampling rates in the MHz range are currently being analysed.

The transport relevance of the measured temperature fluctuations is difficult to estimate. This is due to two facts. First in the experiment described only a restricted range of the k-spectrum of the fluctuations is accessible. The total spectrum and therefore the amount being unknown. Second the poloidal component of the fluctuating E-field necessary to drive a radial transport is completely unknown too. Nevertheless the existence of temperature fluctuations has been proven. Further more detailled parameter scans might give indirect evidence of its transport relevance.

References

[1] P.C. Liewer, Measurements of microturbulence in tokamaks and comparisons with theories of turbulence and anomalous transport, Nuclear Fusion 25 (1985) 543-621

[2] A.J. Wootton et al., Fluctuations and anomalous transport in tokamaks, Physics of Fluids B 2 (1990) 2879-2903

[3] C. Hidalgo et al., Experimental evidence of significant temperature fluctuations in the plasma edge region of TJ-1 tokamak, Phys. Rev. Lett. 69 (1992) 1205-1208

[4] L. Giannone et al., Density, temperature, and potential fluctuation measurements by swept Langmuir probe technique in Wendelstein 7-AS, Phys. Plasmas 1 (1994) 3614-3621

[5] S. Sattler and H.J. Hartfuss, Experimental evidence for electron temperature fluctuations in the core plasma of the W7-AS stellarator, Phys. Rev. Lett. 72 (1994) 653-656

[6] M. Kwon et al., Electron temperature measurements from ECE on TEXT-U, Rev. Sci. Instrum. 63 (1992) 4633

[7] L. Mandel and E. Wolf, Coherence properties of optical fields, Rev. of Mod. Phys. 37 (1965) 231-287

[8] W.B. Davenport and W.L. Root, An Introduction to the Theory of Random Signals and Noise, McGraw-Hill, New York, 1958

[9] R. Loudon, The Quantum Theory of Light, Clarendon Press, Oxford, 1973

[10] R. Hanbury-Brown and R.Q. Twiss, Interferometry of the intensity fluctuations of light, Proc. Royal Soc. A243 (1957) 7-34

[11] J.W. Storey, Far-infrared astronomical spectrometers, Infrared Phys. 25 (1985) 583-

[12] H.J. Hartfuss, Coherent versus incoherent detection schemes, Proc. of the Seventh Joint Workshop and IAEA Technical Committee Meeting on ECE and ECRH (EC-7), Hefei China, 1989, IAEA Vienna Austria, 1990, pp. 267-273

[13] S. Sattler, Fluktuationen der Elektronentemperatur gemessen durch Intensitätsinterferometrie am Stellarator W7-AS, report IPP III/193 of Max-Planck-Institut für Plasmaphysik, Garching, 1993

[13] S. Sattler and H.J. Hartfuss, Intensity interferometry for measurement of electron temperature fluctuations in fusion plasmas, Plasma Phys. Control. Fusion 35 (1993) 1285-1306

[14] G. Cima et al., Core temperature fluctuations and related heat transport in the Texas experimental tokamak-upgrade, Phys. Plasmas 2, (1995) 720-726

[15] H.J. Hartfuss and M. Tutter, Fast multichannel heterodyne radiometer for electron cyclotron emission measurement on stellarator W VII-A, Rev. Sci. Instrum. 56 (1985) 1703-1706

[16] H.J. Hartfuss and S. Sattler, Evidence for temperature fluctuations in the W7-AS stellarator, Proceedings of the workshop on 'Local Transport Studies in Fusion Plasmas', Varenna, Italy, 1993, pp. 305-310

Figure Captions

Fig.1: Spectra of the turbulent fluctuations as measured with the crossed sightline technique at four different radii r/a between 0.53 and 0,75.

Fig.2: The relative fluctuations of the radiation temperature for an ECRH power scan as measured at a plasma radius of 10.6 cm (Fig. 2a). Depending on the phase relation between density and temperature fluctuations, temperature fluctuations as given by the shaded region result. Included is the confinement time (full line). Fig. 2b gives the results for a number of plasma shots at different densities. At low densities the fluctuations decrease with decreasing electron heat diffusivity; to higher densities they increase while the diffusivity is constant in this range.

Fig.3: Two ECE radiometer channels 1 and 2 separated in frequency space overlap in real space (shaded region) due to the finite depth of the emission volume.

Fig.4: The fluctuation level as determined by the different crosscorrelation methods, crossed sightlines (squares), single sightline (dots) (4a). The imperfect overlap of neighboured channels causes the maximum of the crosscorrelation function to occur at finite delay times in the presence of a radial motion of the fluctuating structures (dots). The crossed sightline results scatter around zero delay time (4b).

Fig.5: Installed set-up for combined temperature and density fluctuation measurements consisting of a heterodyne reflectometer and a 2 x 10 channel crossed sightline interferometer both operating with the same Gaussian beam optics.

100
1
0.01
10^{-4}
0
50
100
150
200
250
300
350
f / kHz
$(\tilde{T}_R / T_R)^2$ in a.u. / Hz
noise level
r_{eff} / a = 0.53
r_{eff} / a = 0.60
r_{eff} / a = 0.67
r_{eff} / a = 0.75

Fig. 1

rel. temperature fluct. (%)
100
10
1
0.1
100 200 300 400 500 600 700 800 900
ECRH heating power (kW)
τ_E / ms
20
16
12
8
4
0
• $\tilde{T}_R/T_R$ at r_{eff}=10.6 cm
⋄ $\tilde{T}_e/T_e$ ($\tilde{n}_e$ $\tilde{T}_e$ in phase)
□ $\tilde{T}_e/T_e$ ($\tilde{n}_e$ $\tilde{T}_e$ out of phase)
— τ_E / ms

Fig. 2a

rel. temperature fluct. (%)
10
1
0.1
0
1
2
3
4
5
line integrated density (1019 m-3)

Fig. 2b

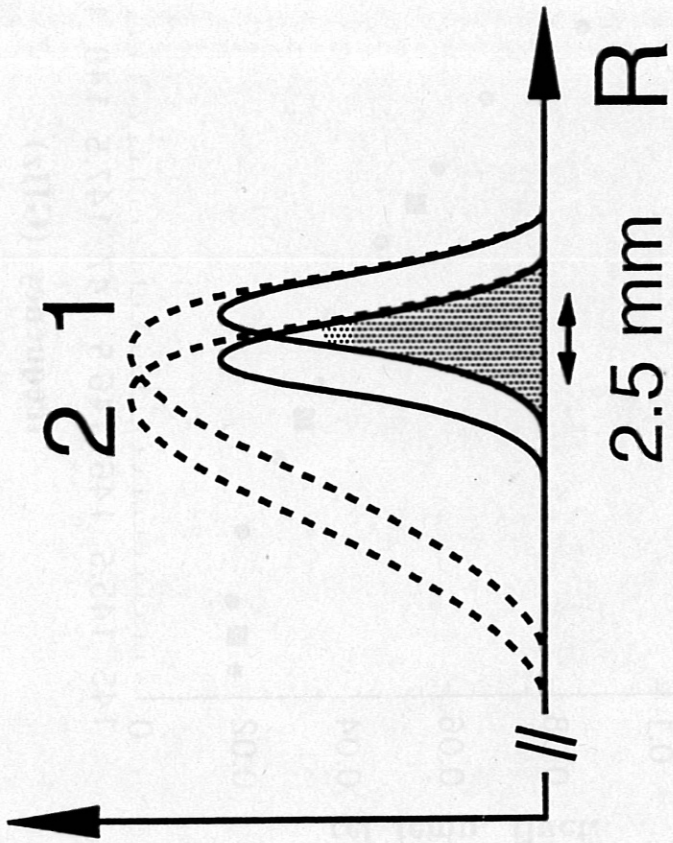

Fig. 3

rel temp. fluct.
0.12
0.1
0.08
0.06
0.04
0.02
0
145
145.5
146
146.5
147
147.5
148
148.5
149
frequency (GHz)

Fig. 4a

time shift (ms)
0.04
0.03
0.02
0.01
0
-0.01
145
145.5
146
146.5
147
147.5
148
148.5
149
frequency (GHz)

Fig. 46

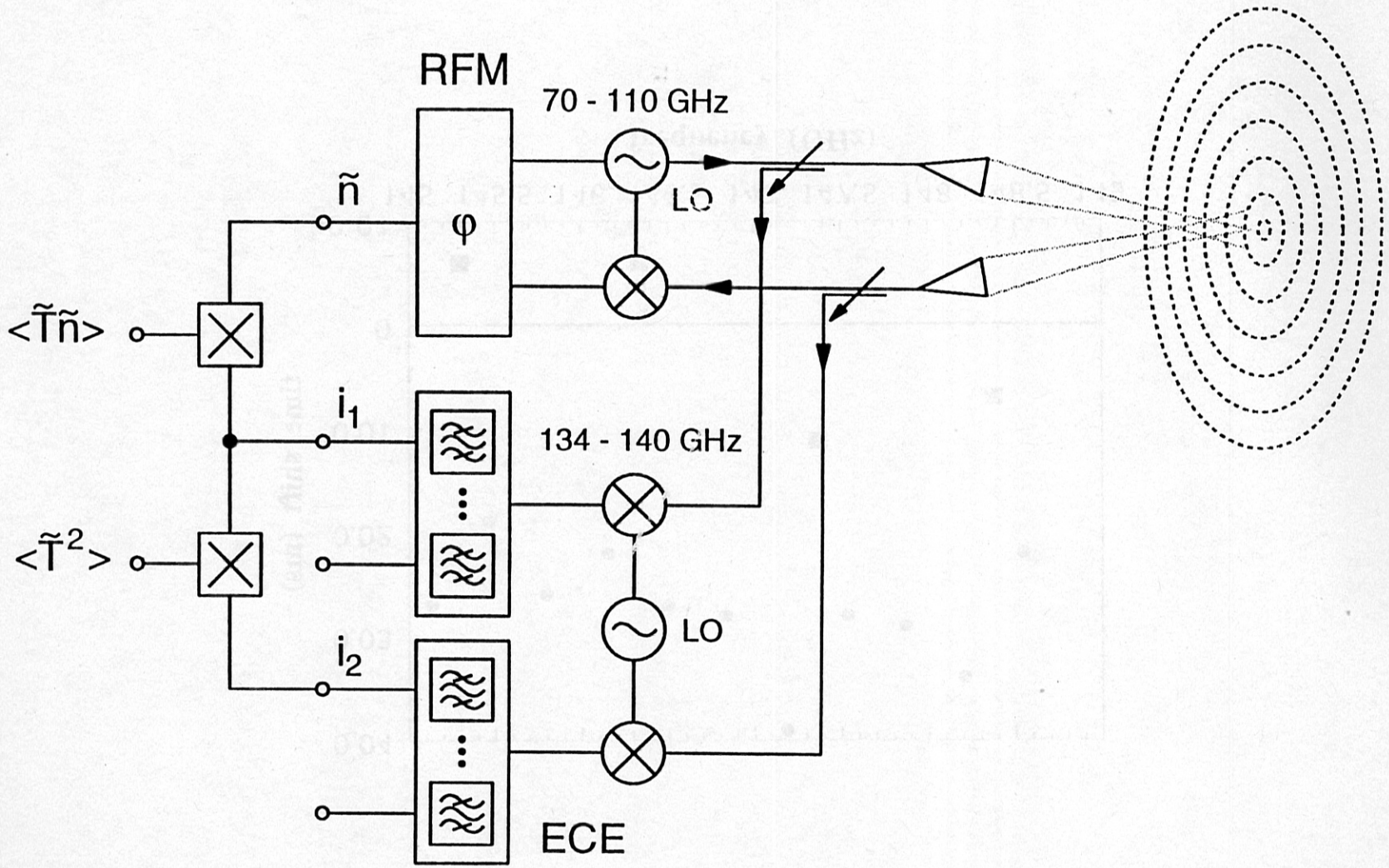
RFM
70 - 110 GHz
LO
$\tilde{n}$
φ
$\langle\tilde{T}\tilde{n}\rangle$
i_1
134 - 140 GHz
$\langle\tilde{T}^2\rangle$
LO
i_2
ECE

OVERVIEW OF W7-X DIAGNOSTICS

M. Kick, H. J. Hartfuss, J. V. Hofmann, P. Grigull, H. Ringler, W7-AS / W7-X Teams

Max-Planck-Institut für Plasmaphysik, Association EURATOM-IPP, D-85748 Garching

Abstract

An overview of the W7-X concept, parameters and planned diagnostics is given. W7-X allows access for all fusion plasma relevant diagnostics, despite of its complex 3-D geometry resulting from the HELIAS (HELIcal Advanced Stellarator) concept and its realization with superconducting coils. Special efforts have been made for diagnostics which are relevant for parameters related to the optimization of the configuration such as reduced Pfirsch-Schlüter currents, very small Shafranov shift, small particle orbit displacement, small change of ι and shear at finite β, reduced neoclassical transport losses in LMFP and plateau, vanishing bootstrap current and good confinement of fast particles at high β. The island divertor concept needs exact local measurements in the divertor region for which suitable diagnostics will be installed.

1. Introduction

Wendelstein 7-X (W7-X) which has been approved for construction in Greifswald / Germany by the Commission of the European Community will be a toroidal magnetic plasma confinement experiment of the HELIAS type, G. Grieger, et al. [1], [2], H. Wobig [3]. It aims at probing the viability of the optimized Stellarator as a desirable fusion power station concept. Operation is scheduled to start in 2004. In order to establish a set of appropriate ports, diagnostic plans have been developed. The geometry of W7-X allows all desired diagnostics for the core and edge of the plasma as well as for the divertor

region to be installed, H. J. Hartfuss and H. Ringler (ed.) [4], J. V. Hofmann et al. [5].

2. Concept, Design, Parameters of W7-X

Following the HELIAS concept [1] the confining magnetic field of W7-X with a helical axis in a five-fold toroidal symmetry is generated by a set of 50 nonplanar superconducting coils arranged in 5 equal toroidal segments (10 sets of only 5 different types of coils), Fig.1. Separate powering of coils of the same type, which are connected in series, gives flexibility concerning the magnetic field topology. An additional set of 20 planar coils (4 per module, not shown in Fig.1) allows variations of the axis position as well as of the rotational transform on axis and at the boundary from $0.75 \leq \iota(0) \leq 1.01$ and $0.83 \leq \iota(a) \leq 1.25$, respectively. The plasma cross section varies from bean-shaped at the position of strongest curvature ($\Phi = 0^o$) via drop-like ($\Phi = 18^o$) into triangular in the region of smallest curvature ($\Phi = 36^o$), Figs.1, 2.

The design of W7-X follows the optimization criteria of the HELIAS concept [1]. The strong reduction of the averaged toroidal curvature results in strongly reduced Pfirsch-Schüter currents, very small Shafranov shift and orbit displacement, see Fig.2, good fast particle confinement at high β and very small bootstrap currents. The improved magnetic field topology, with few Fourier components only, is predicted to reduce significantly neoclassical transport losses in the plateau as well as in the LMFP region. The magnetic surfaces are smooth and due to the low shear without low order islands in the confinement region.

W7-AS already demonstrated the technical feasibility of a nonplanar modular coil system. W7-X shall prove the viability of this concept with superconducting coils [2].

Particle and energy exhaust under stationary conditions are major objectives of W7-X in order to develop a suitable divertor system [4], [6].

Major and averaged minor radii will be 5.5 m and 0.53 m, respectively. With $B \leq 3T$ and heating powers of 10 MW of ECRH, cw, 4.5 - 18 MW (in a later operational stage) of NBI, 10 s and 4 - 12 MW of ICRH, 10 s, the following maximum plasma parameters are predicted: $T_e \leq 10$ keV and $T_i \leq 8$ keV, densities up to $3 \cdot 10^{20}$ m^{-3} and $\langle\beta\rangle \leq 4.5\%$. The power load of the divertor plates is expected to be less than 10 MW/m^2 [1], [4], [6].

3. W7-X Diagnostics

The geometrical structure with the superconducting coil system allows to install a large number of reasonably big ports for heating and diagnostics. Because of the five-fold symmetry there are 10 times as much ports available as shown in Fig.3, with some restrictions only concerning the symmetry planes of port A1, $\Phi = 0^o$, and the tangential ports, Q1, close to NBI. Due to the large aspect ratio there will be ports also on the inboard side of the torus.

All basic diagnostics, which are well known from other fusion research devices, are compatible with the port geometry of W7-X and are planned to be installed: Thomson scattering: for $T_e(r)$ and $n_e(r)$; ECE (**E**lectron **C**yclotron **E**mission) for $T_e(r)$; active CX (**C**harge e**X**change) neutral particle analysis: for $T_i(r)$ and slowing down spectra of high energetic particles; CXRS (**CX R**ecombination **S**pectroscopy): for $T_i(r)$, $n_{imp}(r)$, $v_{pol/tor}$, $E_{rad}(r)$; interferometry and polarimetry: for n_e; reflectometry and fast Lithium beam: for $n_{e,edge}$; spectroscopy in different wavelength ranges, bolometry and PHA (**P**ulse **H**eight **A**nalysis): for plasma radiation, impurities and Z_{eff} ; H_α-diagnostic: for

neutral particle density and recycling; soft-X, magnetic measurements and probes: for T_e, fluctuations, MHD instabilities; diamagnetic and flux loops: for energy content and plasma currents; edge probes: for n_e, T_e and Φ; calorimetry: for heat load; plasma and infrared video: for plasma configuration, monitor and heat load. Microwave scattering, LENA (**L**ow **E**nergy **N**eutral particle **A**nalysis), collective Thomson scattering (at e.g. 140 GHz) and neutron measurements as well as an in situ measurement of the magnetic flux surfaces by an electron beam are foreseen [4].

Special efforts have to be made for the measurement of quantities directly related to the optimization of W7-X, as stability, equilibrium, confinement and transport:

For the soft X-ray diagnostic a system of 3 pinhole cameras at $\Phi = 23^0$ which covers the complete plasma cross section as well as the divertor and a tomographic system with 12 -15 compact cameras inside the vessel at $\Phi = 36^0$ will be installed. Probe arrays and video diagnostics are foreseen for measurements of the edge topology of the plasma. Axis position, plasma radius and Shafranov shift, the reduction of which is a direct proof of the optimization, are thus accessible. MHD activities, the identification of mode structures, possible operational limits due to MHD instabilities and the check of predicted instability thresholds are aims of these measurements [4].

An improvement of transport by a factor of about 10, both in the plateau and LMFP region, compared to an axisymmetric configuration is neoclassically predicted for the optimized configuration of W7-X due to a strong reduction of the averaged toroidal curvature. In different magnetic configurations, generated e.g. by varying the mirror ratio, neoclassical transport properties can be influenced, thus allowing to check theoretical

predictions. For local transport analysis accurate measurements of the T_i, E_{rad}, T_e and n_e profiles are required. As an example the geometry of active CX and CXRS is shown in Fig. 4. Thomson scattering, ECE, interferometry / polarimetry, reflectometry and a fast Lithium beam will also be available. A feasibility study for a heavy ion beam probe is presently carried out. Thus neoclassical transport properties as well as confinement transitions, changes of the electrical field, the temporal behaviour of injected particles or the distribution of impurities can be investigated [4].

A good fast particle confinement is predicted for W7-X for $\langle\beta\rangle \geq 2\%$. The investigation of the confinement of simulated α-particles needs the development of new diagnostics. The slowing down of 60 keV deuterons in W7-X corresponds to 3.5 MeV α-particles on power station scale (equal a/ρ). Supporting calculations of the deposition of fast particles from neutral particle beams (NBI or diagnostic beam) or from ICRH minority heating are needed. Comparison with measurements of, e.g. slowing down spectra by NPA, see also Fig. 4, resonance fluorescence of sputtered impurities or deposition probes, can be made [6].

Because of the known structure of the magnetic field the transformation between geometric and magnetic coordinates is available for all relevant configurations of W7-AS by the TRANS code an extension of which to the higher dimensional parameter space of W7-X is straight forward, F. Sardei in [4]. Mapping of experimental data can thus be obtained for any toroidal and poloidal position. A different approach to this problem are fast equilibrium calculations using function parameterizaton, P. J. Mc Carthy in [4]. Investigations are underway if these are able to give a sufficiently good set of different

scenarios for W7-AS for comparison to real experimental parameters.

4. W7-X Divertor

For particle and energy exhaust of W7-X an open divertor configuration will be designed in a first step. The island divertor concept makes use of the existence of large islands at the boundary in magnetic configurations with moderate shear. Streaming along the field lines the plasma passes the island separatrix and gets to the outermost region of the island with typical magnetic connection lengths of 100 - 300 m. Due to finite β effects an ergodization of magnetic field lines at the boundary occurs which can be enlarged for certain values of ι by superimposing additional stationary magnetic fields. The target plates, intersecting the island, follow the helical edges and are appropriately shaped in order to decouple the plasma from the vessel wall and to minimize the local wall load ($P_{max} \leq 10$ MW / m^2). They are made to cover the whole ι-range from 5/6 to 5/4 with different sizes and positions of islands and the ergodic boundary layer, Fig. 5. The importance of the knowledge of the edge structure of the W7-X configuration for divertor operation requires exact local measurements in this region. The divertor region will be accessible for diagnostics by special ports parallel to the target plates in $\Phi = 13.5^{\circ}$ planes. It will be equipped with Thomson scattering, laser induced fluorescence, target integrated retractable Langmuir probe arrays, reciprocating probes, He beam, fast Lithium beam, microwave diagnostics, video, spectroscopy and neutral gas diagnostics. Thermography will be installed in a different position, viewing upper and lower divertor plates from different ports [4], [6].

Steady State Operation

Special diagnostic problems may arise because W7-X will be capable of steady state operation. Most experiments, however, will be done in pulsed operation of several minutes with ECRH and 10 seconds with NBI or with ECRH, cw, with periodic NBI pulses of 10 s. On the one hand intelligent event recognition will be needed because of limited data aquisition capacity, but long integration times on the other hand may give access e.g. to improved correlation measurements. Slow scans of diagnostics may enable profile measurements with good spatial resolution even with a reduced number of spatial channels. Experience of other experiments, especially Tore Supra, will be incorporated as well as developments for LHD. The EURATOM Associations have been invited to take part in development and operating of different diagnostics. Fields of interest have been defined so far and possible contributions have been considered in the application to EURATOM for preferential support, phase II. The data acquisition system is also planned to be realized jointly [6].

[1] G. Grieger et al., Physics and engineering studies of W7-X, in Proceedings of 13th International Conference on Plasma Physics and Controlled Nuclear Fusion Research, Washington (1990), IAEA,Vienna, 1991, p. 525 ff.

[2] G. Grieger et al., Physics Optimization of Stellarators, Physics of Fluids, B 4, 1992, p. 2081 ff.

[3] H. Wobig, The Theoretical Basis of a Drift Optimized Stellarator Reactor, Plasma Physics and Controlled Fusion, 35, 1993, p. 903 ff.

[4] H.J. Hartfuss and H. Ringler (ed.), Proceedings of the International Workshop on W7-X Diagnostics, Ringberg Castle, Germany, 1995

[5] J. V. Hofmann et al., in Diagnostics for ITER, Proceedings of the International Workshop, Varenna, 1995, Plenum, New York , to appear

[6] Wendelstein Project Group, W7-X Application for Preferential Support, Phase II, Garching, Germany, 1994

Figure 1: Part of the modular coil set and 3-D plasma surface for rotational tranform $\iota = 1$. The plasma has a helical axis and its cross section varies from bean shaped at $\Phi = 0^{o}$, via drop like at $\Phi = 18^{o}$, to triangular at $\Phi = 36^{o}$.

Figure 2: Comparison of poloidal plasma cross sections at $\Phi = 0^{o}$ (left), $\Phi = 18^{o}$ (center), and $\Phi = 36^{o}$ (right), respectively, for $\beta = 0$ (upper) and $\beta = 5\%$ (lower line). The effect of finite β on the flux surfaces is very small.

Figure 3: 3-D plot of about half a torus module (1/10 of entire torus) and ports, $\Phi = 0^{o}$ at center of port A1, $\Phi = 36^{o}$ at center of port U1.

Figure 4: Diagnostic neutral particle beam (**D**iagnostic **I**njector, DI) for active **C**harge e**X**change (CX) **N**eutral **P**article **A**nalysis (NPA) and **C**harge e**X**change **R**ecombination **S**pectroscopy (CXRS) in poloidal cross section, (toroidal active CX and CXRS will be possible via port Q1, see Fig.3). The DI penetrates the plasma horizontally from the out-board (K1) to the inboard (L1) side. In the poloidal plane an array of 5 NPA, the lines of sight of which can be scanned across the plasma, and 2 (core and edge) multichannel CXRS lines of sight, port NEW1, are viewing the beam. The equivalent geometry (in different modules) will be used for Thomson scattering, laser blow off, and pellet injection.

Figure 5: W7-X divertor shown in poloidal plane, $\Phi = 9^{o}$.

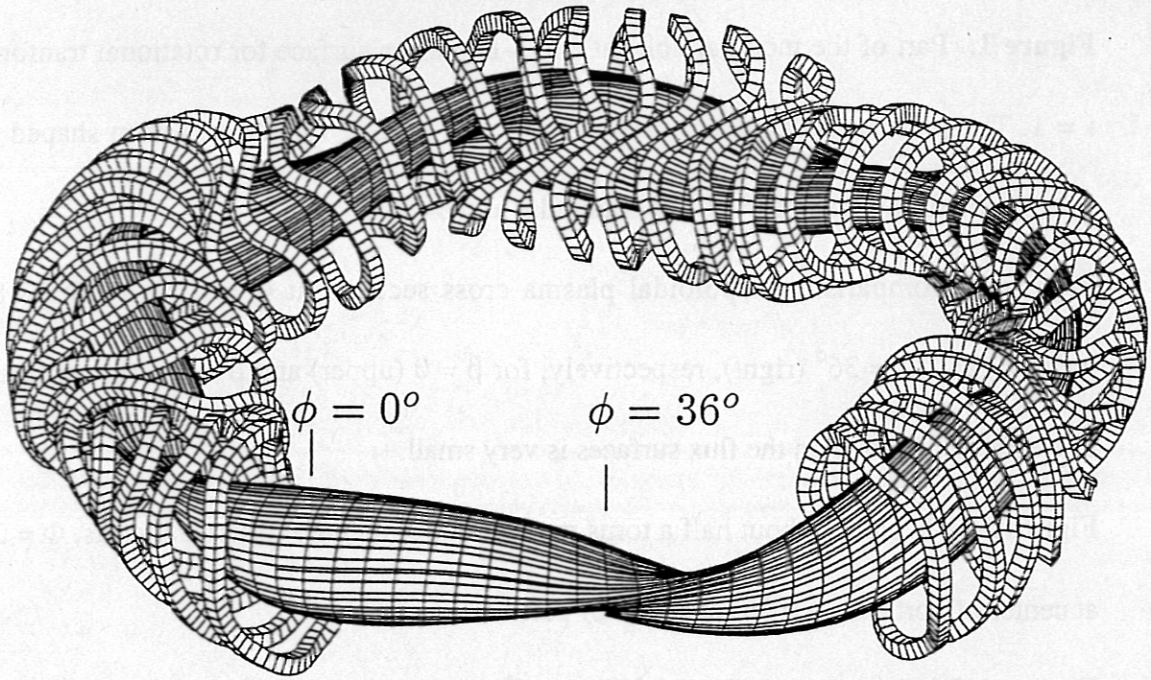

M. KICK, ITC-7, L1-01 (ORAL) FIG. 1

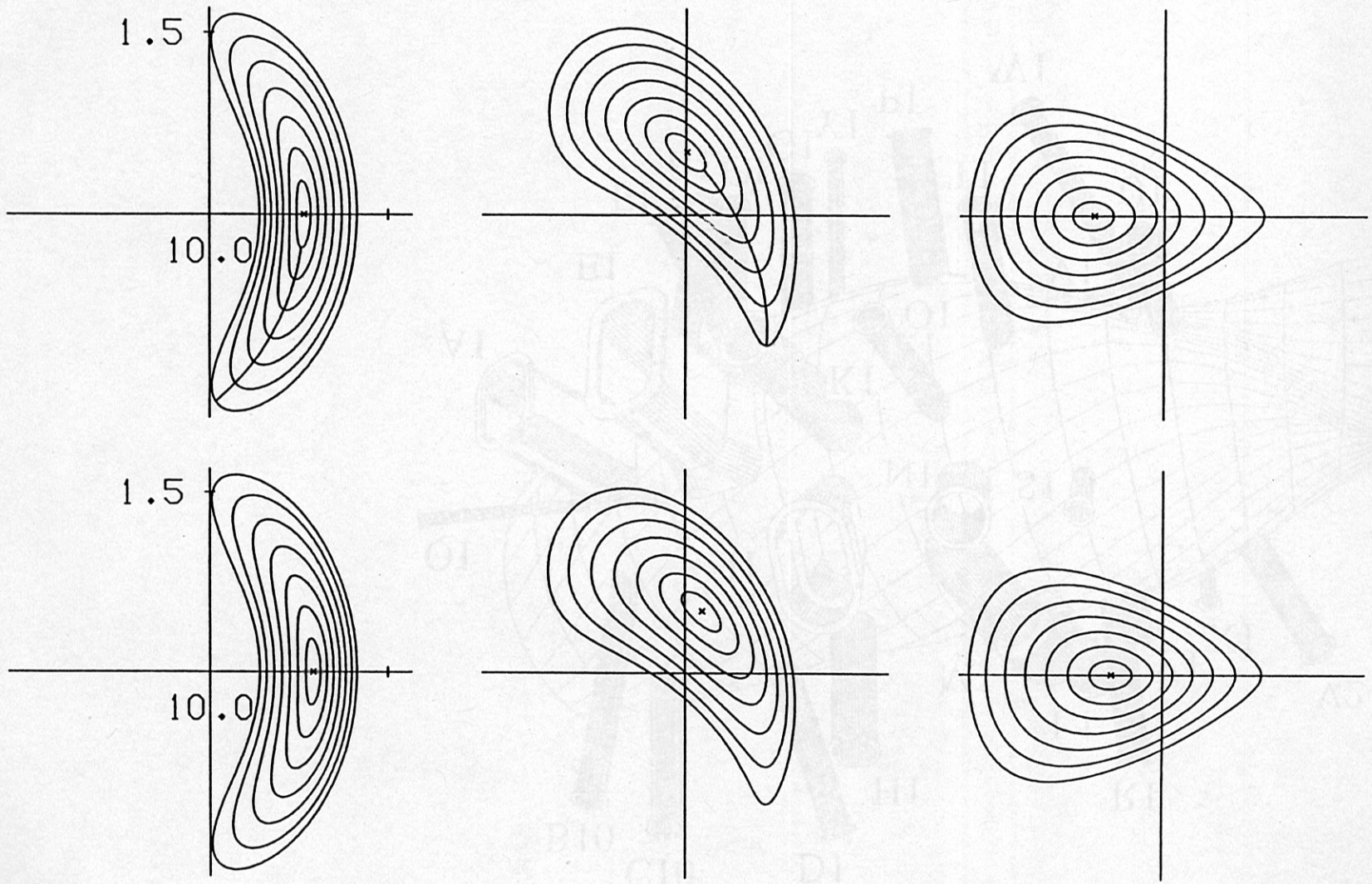

M KICK, ITC-7, L1-01, ORAL

FIG. 9

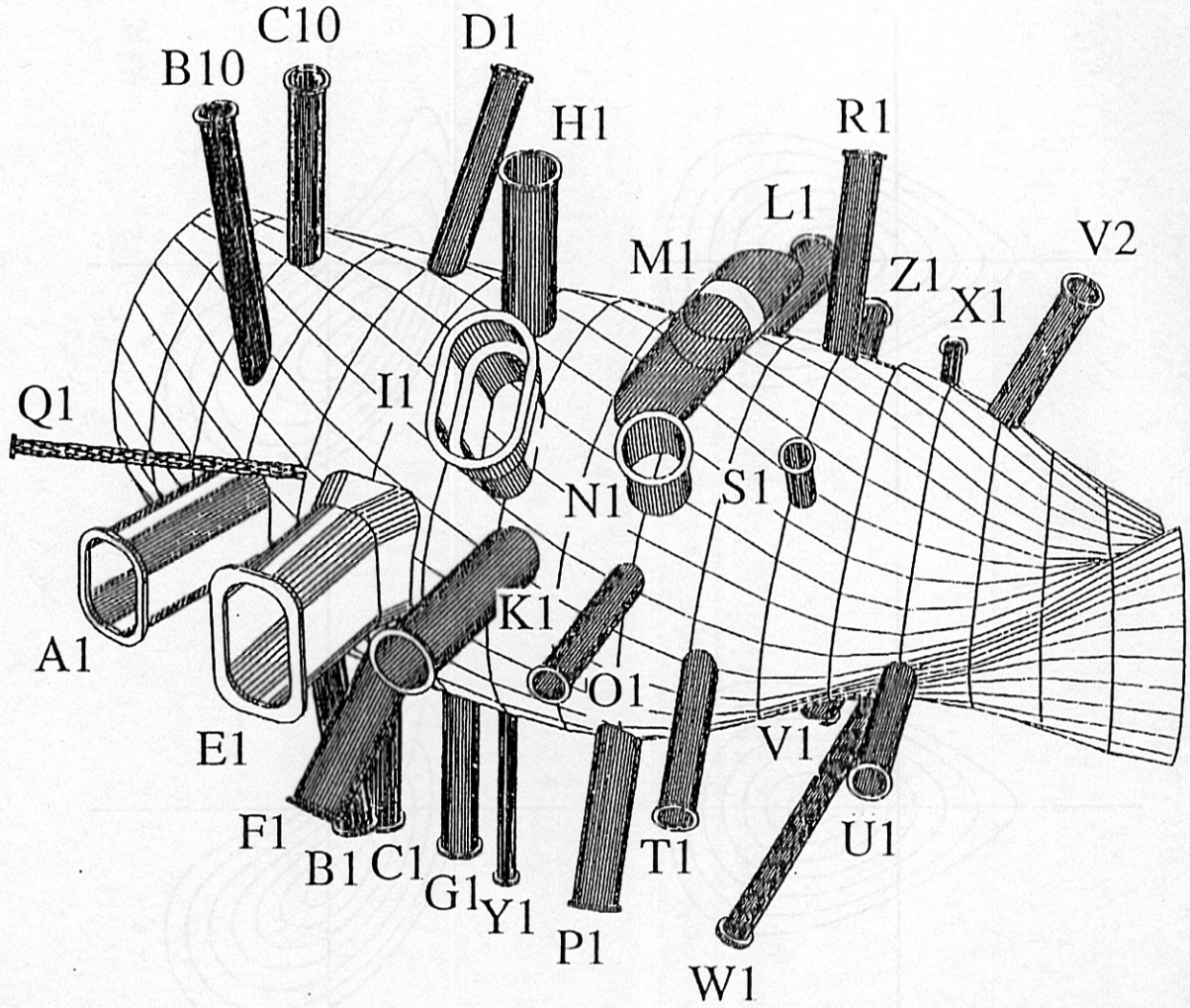

M. KICK, ITC-7, L1-01, (ORAL)

FIG 3

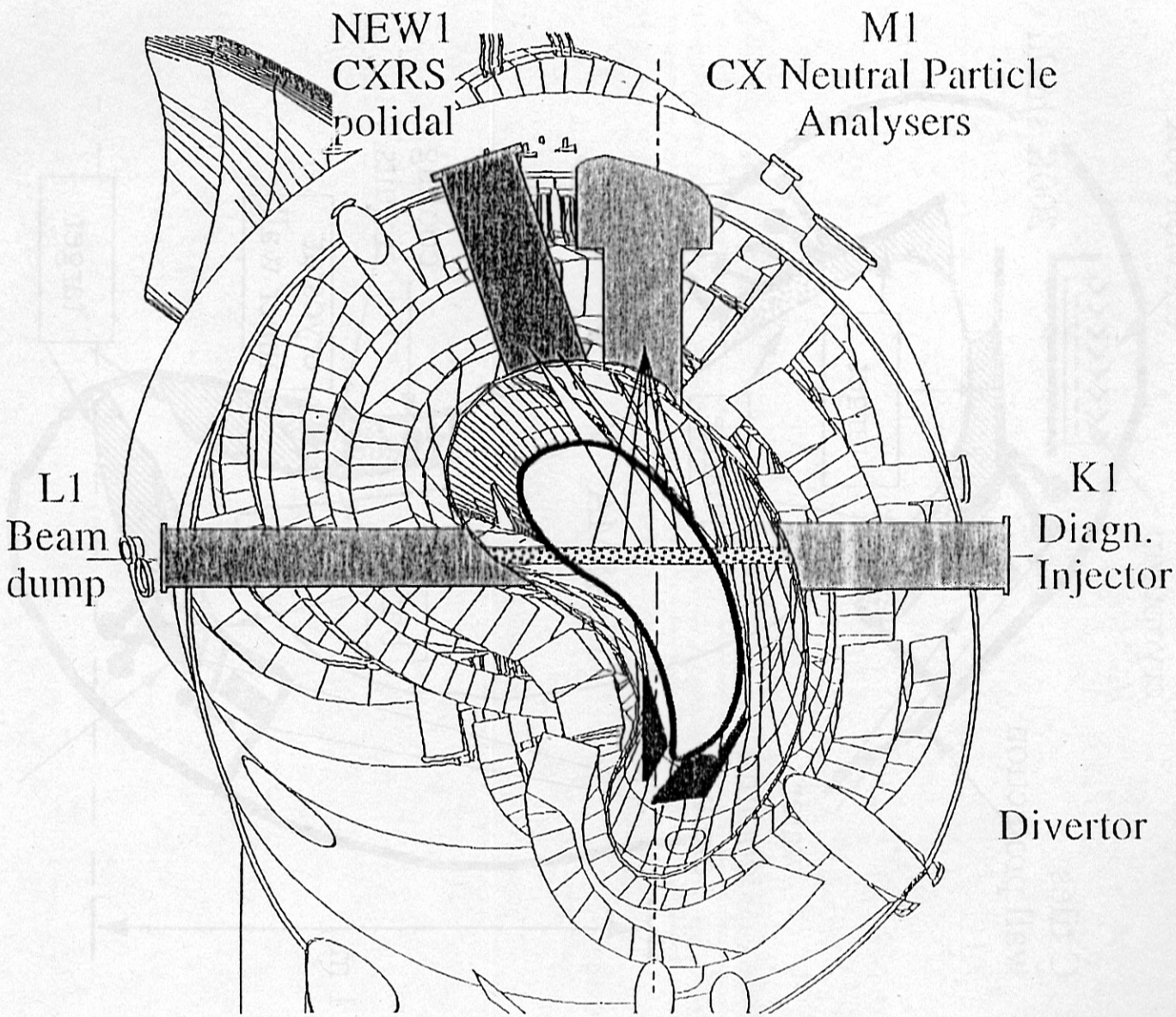
NEW1
CXRS
poloidal
M1
CX Neutral Particle
Analysers
L1
Beam
dump
K1
Diagn.
Injector
Divertor

Fig. 4

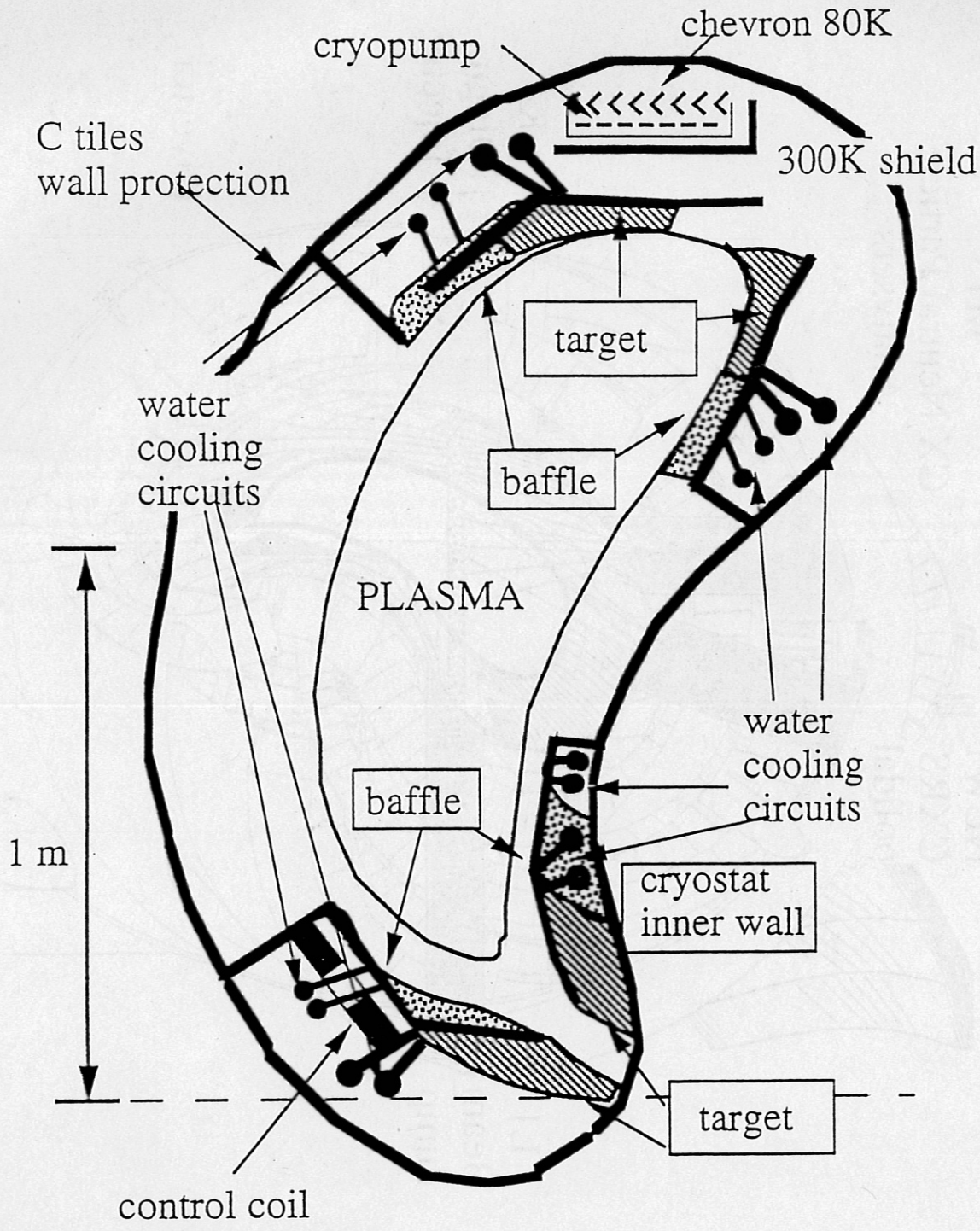

M. KICK, ITC-7, L1-01 (ORAL)

FIG. 5

PLASMA DIAGNOSTICS AND PHYSICS IN THE W7-AS STELLARATOR

A. Weller, J. Baldzuhn, R. Brakel, R. Burhenn, V. Erckmann, Y. Feng, S. Fiedler, J. Geiger, L. Giannone, P. Grigull, H.J. Hartfuss, M. Hirsch, J.V. Hofmann, M. Kick, C. Konrad, H. Maassberg, N. Rust, F. Sardei, E.V. Suvorov[1], W7-AS Team, ECRH Group, NBI Group, ICRH Group

Max-Planck-Institut für Plasmaphysik, EURATOM Association,
Boltzmannstr. 2, 85748 Garching, Germany,
Fax: 089 3299 2584, e-mail: weller@ipp-garching.mpg.de
[1]Inst. of Applied Physics, Nizhniy Novgorod, Russia

ABSTRACT

A survey of experimental techniques and analysis tools used at W7-AS for the investigation of the equilibrium, stability, transport and edge plasma is given, and examples for typical results are presented. The emphasis is on measurements, which are particularly relevant for the investigation of stellarator specific issues including the characterization of different magnetic configurations with respect to equilibrium, stability and transport, and the identification and verification of stellarator optimization elements. Another important field is the diagnostics of the 3-dimensional plasma edge under various conditions. In particular, the exploitation of boundary islands for use as an „island divertor" and for the establishment of a radiating island chain are important issues closely linked with the problems of power exhaust and particle control in steady state devices. The plasma edge topology also has a great impact on the achievement of the H-mode regime. The stellarator also offers the possibility to perform specific physics studies such as profile shaping experiments or the investigation of bootstrap currents, of electron cyclotron current drive and power deposition, and of the influence of magnetic shear and islands on transport and stability.

1. INTRODUCTION

WENDELSTEIN 7-AS is a low shear, modular stellarator (R = 2m, $a \approx 0.17$ m, 5 field periods). W7-AS has some flexibility to change the configuration with respect to rotational transform, the magnetic ripple and the plasma position by using the independent power supplies in the additional planar coils, the modular „corner coils" (Fig. 1) and the vertical field coils, respectively. In fig. 2 some of the investigated configurations are shown, characterized by the magnetic field strength along the plasma axis over one field period. The usual operation of W7-AS is with zero toroidal net current, where the internally driven toroidal currents (e.g. bootstrap currents) are compensated by use of the OH transformer in order to control the edge rotational transform. The ECRH system is being upgraded by changing from a 70 GHz system (2.5 T, O1-mode or 1.25 T, X2-mode, presently < 0.5 MW, 3s) to an 140 GHZ system (2.5 T X2-mode, presently < 1MW, 1.1 s). Also the neutral beam injection system (NBI) was upgraded to provide about 3 MW injected power (45-55 keV H, D and He, 2 injectors, almost tangential, in co- and counter direction). Target plasmas for NBI are either produced by ECRH (at 1.25 T or 2.5 T) or by a 900 MHz magnetron system, which allows to change the magnetic field in a wide range. Recently first successful ICRH experiments have been performed (H-minority heating at 2.5 T, 38 MHz, < 0.3 MW coupled to the plasma).

The physics programs presently concentrate on the extension of the parameter range, accessible with the increased heating power, in combination with a proper choice of the magnetic configuration (Jaenicke et al. [1]). In order to cope with the increased heat loads extensive plasma edge studies were performed to develop an island divertor concept.

2. MAGNETIC CONFIGURATIONS, EQUILIBRIUM AND STABILITY

Toroidal equilibria (including net current-free cases) give rise to currents according to $\mathbf{j} \times \mathbf{B} = \nabla p$. In addition to the diamagnetic currents $j_\perp$ the condition $\nabla \cdot \mathbf{j} = 0$ requires

parallel currents $j_{\parallel}$ (Pfirsch-Schlüter currents), which lead to the outward shift of the magnetic surfaces (Shafranov shift). This effect not only gives rise to an equilibrium beta-limit, but also reduces the stability limit by introducing destabilizing terms depending on the parallel current density into the Mercier and resistive interchange criteria. In addition, neoclassical transport effects are larger in the presence of significant $j_{\parallel}$ due to the component of the guiding center drift out of the magnetic surface. Particularly in the case of low shear stellarators the Pfirsch-Schlüter currents can lead to relatively large changes of the rotational transform profile generating unwanted rational surfaces inside the plasma. Therefore, the reduction of these currents can lead to an optimization in various respects. In W7-AS the ratio $\langle j_{\parallel}/j_{\perp}\rangle^2$ is reduced by a factor of about 2 compared with an equivalent conventional stellarator configuration. Thus, a main issue in W7-AS is to verify the corresponding improvements in the equilibrium and neoclassical transport properties (e.g. reduced Shafranov shift to demonstrate the benefit expected from more advanced stellarator configurations such as W7-X (Nührenberg et al. [2]).

Experimental data on the plasma position (axis and boundary) is obtained from soft X-ray profile measurements, from Thomson and ECE data, Langmuir-probes and magnetic loops. Fig. 3 shows the plasma shift derived from X-ray profiles, obtained for a set of NBI heated shots. The data are separately given for the two main operational regimes ($\iota \approx 1/3$ and 1/2). The shift is clearly reduced with respect to predictions for the conventional $l = 2$ stellarator configuration (full lines). In particular cases tomographic reconstructions of X-ray data from 2 X-ray arrays were obtained by using dfferent codes. The evaluated X-ray emissivity distributions are generally in good agreement with the corresponding equilibria as calculated by the VMEC/NEMEC code (S.P. Hirshman et al. [3]).

At 1.25 T $\langle\beta\rangle \approx 1.8\%$ was achieved ($\beta_0 \approx 4\%$) with NBI. In this case the calculated equilibrium surfaces show a substantial Shafranov shift, which leads to an increase of shear and the appearance of low order rational surfaces inside the plasma (fig. 4). In this

β-range, resistive interchange unstable regions are predicted in the outer part of the plasma, particularly for inward shifted configurations. In these cases, where the vacuum magnetic well depth ensuring stability at low β (low shear) is reduced, bursts of MHD activity accompanied with profile relaxations and small drops of the plasma energy were found in signals of Mirnov coils and X-ray diodes. Coherent low frequency ($\leq$ 8kHz) oscillations, which do not influence the global confinement, already appear at lower β with mode numbers consistent with rational values in the ι-profile. They are usually not seen by magnetics, and their mode structure is analyzed by X-ray simulations.

A particular class in the observed MHD activity are Shear Alfvén instabilities driven by fast NBI ions in the lower β-regime. In stellarators with very weak shear low-n TAE modes as found in tokamaks do not occur, but Global Alfvén Eigenmodes (GAE) inside gaps below the shear Alfvén continua (Weller et al. [4]). These modes are detected by various diagnostics, including soft X-rays, ECE, reflectometer and Mirnov coils, as very coherent oscillations in the range 15-70 kHz (fig. 5). The mode characteristics (fast particle drive, frequency, direction of propagation and the radial and poloidal mode structure) is in agreement with theoretical predictions. In particular cases of bursting modes some evidence of mode induced fast particle losses were indicated by drops in the neutron flux (from D injection) in correlation with the MHD activity. At present investigations are underway to study the Alfvén spectrum and the damping mechanism by launching waves with an external antenna.

3. STUDIES OF THE CORE PLASMA AND TRANSPORT

For the measurement of transport relevant plasma parameters in the core Thomson scattering diagnostics (ruby laser and Nd:YAG system), HCN- and μ-wave interferometers, neutral particle analyzers, spectroscopic diagnostics (in particular CXRS) are used. Time dependent measurements of T_e are available from the ECE system and from the X-ray two-foil method.

The most dominant effect for optimizing the neoclassical confinement properties of a magnetic configuration is determined by the average toroidal curvature, which is reduced in W7-AS by a factor of about 0.7 leading to an improvement of the neoclassical transport coefficients by a factor of 2 both in the plateau and the LMFP regimes. A moderate increase of the currents in the large special coils located in the region of the strong toroidal curvature (by up to 20%) leads to a configuration with minimum variation of B at the plasma axis (dashed curve in fig. 2), and the transport in the LMFP regime is further reduced by a factor of about 2. A fairly equivalent improvement is predicted for inward shifted configurations with about $B_z/B = 0.01$ (fig. 6 and lower solid curve in fig. 2). Under these conditions, with combined heating (≈ 0.8 MW NBI and ≈ 0.4 MW ECRH) the ion temperature could be raised up to $T_i \approx 1.6\,\mathrm{keV}$ ($T_e \approx T_i$) as measured by neutral particle analyzer in combination with a diagnostic neutral beam. With increasing NBI power the density cannot be sufficiently controlled. This leads to a decrease of the ion temperature, since the ion heat conductivity and the collisional power transfer to the electrons are increased at higher collisionality.

The neoclassical transport in the LMFP and plateau regimes of stellarators is crucially depending on the magnetic field ripple and the magnitude of the ambipolar radial electric field (fig. 6). Therefore, the determination of E_r is required for the verification of the neoclassical theory. This is achieved in W7-AS by spectroscopic measurements of the poloidal and toroidal plasma rotation velocities using a pulsed diagnostic neutral beam injector, which excites charge exchange recombination radiation of Helium (He II, 4686 Å, ≈ 1% He from initial gas puff). From the CX line intensity, Doppler broadening and shift, the He concentration profile, the ion temperature and the plasma rotation velocity profiles are evaluated. Then E_r is calculated from the simplified radial momentum balance equation:

$$E_r = \frac{\partial(k \cdot n_{He} \cdot T_i)/\partial r}{e \cdot n_{He} \cdot Z_{He}} - \left(V_\theta B_\phi - V_\phi B_\theta\right)$$

As an example the measured radial electric field by spectroscopy (dots) and Langmuir probes (circles) are shown in fig. 7 versus the minor radius. In most cases the observed electric fields correspond to the ion root ($E_r < 0$) and lead to a substantial reduction of the neoclassical ion heat conductivity with respect to the case $E_r = 0$ (fig. 6).

Poloidal and toroidal rotation have also been measured from Doppler shift of active charge exchange excited C^{5+} and passive B^{3+} spectral line emission in the center and near the peripheryof the plasma, respectively. A characteristic change of the poloidal rotation at the plasma edge was observed, as in other devices, in correlation with transitions into H-mode (or back transitions) (Wagner et al. [5]). Studies of the toroidal rotation were particularly performed for configurations with different magnetic field ripple as introduced in fig. 2. Different scenarios involving co-, counter- and balanced NBI were investigated. It could be shown, that the viscous damping of the toroidal rotation is strongly increased in the case of higher field ripple. In this case damping due to the toroidal parallel viscosity is dominant and reasonable agreement is found with neoclassical theory. In the standard configuration the toroidal parallel viscosity is not sufficient to explain the observed rotation velocities and contributions from perpendicular viscosity have to be taken into account (Hofmann et al. [6]).

The influence of the magnetic ripple on losses of fast injected ions is another important issue. Enhanced losses of almost perpendicularly injected ions (diagnostic beam) are clearly evident in CX signals for configurations with increased magnetic ripple. However, no clear effect was found comparing slowing down spectra of particles injected almost tangentially with the heating beams.

4. SPECTROSCOPY AND IMPURITY TRANSPORT

W7-AS is equipped with a set of complementary diagnostics for the determination of the impurity content and for impurity transport investigations. Two laser blow-off systems (LBO) allowing to inject metals evaporated from thin films or micropellets are available for transport studies. The penetration and deposition can be monitored by

visible light spectrometers, which additionally allow to determine the fractions of neutral atoms and clusters. This composition, which influences the deposition profile, can be controlled by the film thickness and the laser power density. From the temporal evolution of spectral line radiation from different ionization states (Al IX-XIII, Fe XVI-XXI), as measured by the crystal spectrometer and the X-ray cameras, information about the impurity transport is derived by means of the transport and radiation code SITAR (W7-A Team,[7]). A statistical analysis of the impurity confinement time in ECRH plasmas with $n_{e0} \leq 5 \cdot 10^{19}$ m^{-3} (Burhenn et al. [8]) gives a scaling according to

$$\tau_{Al}[\mathrm{ms}] = 4.6 \cdot 10^{2}\ a_p[\mathrm{m}]^{2.4\,(\pm 0.4)}\ B_0[\mathrm{T}]^{0.3\,(\pm 0.2)}\ P[\mathrm{MW}]^{-0.8\,(\pm 0.2)}\ n_{e0}[10^{19}\mathrm{m}^{-3}]^{1.2(\pm 0.2)}$$

which shows a similar trend as the global energy confinement, with $\tau_{Al} \approx 4\tau_E$. However, the dependence on the rotational transform and in addition on the working gas (H,D) and Z_{eff} is not yet clear.

Impurity transport investigations were also done using a gas-oscillation technique, where gaseous impurities (e.g. H_2S for S, F_3CH for F) were injected by a sinusoidal modulated gas valve (5-10Hz) during the stationary phase of the plasma discharge (Unger [9]). Transport parameters can then be determined by a phase and amplitude analysis of the radially propagating impurity wave, which is monitored by the X-ray cameras (He- and H-like ions) using suitable absorber foils to minimize the background radiation (fig. 8).

At medium densities the experimental data are in agreement with simulations based on neoclassical theory within the error bars. For the lowest density enhanced values for the diffusion coefficients are required to simulate the data. At the highest density, however, the neoclassical fluxes had to be reduced by factors of 4-10 to get agreement with the experimental data, which is not yet understood and subject to further investigations.

5. STUDIES WITH ECRH/ECCD

Heat diffusivity studies using heat waves have been conducted in the W7-AS under a variety of plasma conditions and heating scenarios (Hartfuss et al. [10]). The heat wave

is generated by modulating the ECRH power, introducing a small temperature perturbation (< 10%) whose radial propagation away from the power deposition zone is studied by means of a 24 channel ECE heterodyne radiometer. Both, the phases and the amplitudes of the heat wave are taken into account in the analysis. It was found that the diffusivity determined in modulation experiments agrees within the error bars with the heat diffusivity as determined from stationary power balance analysis in W7-AS. In the course of these experiments and parameter studies, the modulation frequency, f_{mod}, was varied in the range between 20 Hz and 10 kHz. The decay length of the heat wave decreases at high modulation frequencies according to $\lambda = \sqrt{\frac{2\chi}{3\pi f_{mod}}}$ (Hartfuss et al. [11]). The temperature modulation profile then approaches the power deposition profile. An example for the measurements is shown in fig. 9, where the width (FWHM) of the temperature modulation profile is plotted against the modulation frequency for 2 gyrotrons, which differ by their beam width. From extrapolation to high frequencies the different power deposition profiles can be determined

We have investigated the influence of a local shear modification on the confinement by inferring well localized currents with Electron Cyclotron Current Drive (ECCD). A two-frequency ECRH system at 70 (0.4 MW) and 140 GHz (0.7 MW) both with an optical low field side launch provides a flexible tool for on- and off-axis current drive in a wide plasma parameter range (Erckmann et al. [12]). The experiments were performed with an inductive compensation (OH-transformer feedback) of both the bootstrap and the EC driven current, i.e. the EC driven current component was changed by scanning the launch angle of the incident microwaves while keeping the plasma net current zero. In a second experiment the EC-resonance layer was scanned across the plasma cross section at a fixed oblique launch angle, i.e. the radial position of the EC-driven current was scanned while maintaining a fixed edge value of the rotational transform at zero net current. A strong response of the global confinement on the internal current density distribution was measured in narrow parameter windows which is attributed to the change of the internal rotational transform. For some cases the measured confinement

degradation correlates with the appearance of major magnetic resonances in the plasma cross section, which is accompanied by coherent MHD activity. The enhanced transport across perturbed regions can produce shoulders in the T_e profiles and is also seen in phase and amplitude profiles of heat waves (fig. 10). Optimum confinement is obtained for flat iota profiles avoiding resonances.

The assessment of ion temperatures and fast ion velocity distributions by Collective Thomson Scattering (CTS) using μ-waves was studied in W7-AS. For the first time experiments were performed with a 140 GHz gyrotron (≈ 0.45 MW) at 1.25 T (Suvorov et al. [13]), where the ECE background (at 4th harmonic for 140 GHz) is of the order of a few eV only. The ion feature was measured in the parameter range of 0.4 10^{20} m^{-3} < n_{eo} < 0.9 10^{20} m^{-3} and 0.3 < $T_e \approx T_i$ < 0.5 keV in NBI-heated discharges with tangential injection. The measured spectra are well represented by theoretical modeling as shown in fig. 11. Operation at 2.5 T (2nd harm. at 140 GHz) is characterized by a strong ECE background and resonant absorption of incident and scattered radiation. The scattered spectra show a broad nonthermal feature in the frequency range < 0.5 GHz where the ion line is expected. The additional injection of a perpendicular 22 keV neutral beam destabilizes a lower hybrid wave, which is clearly detected by CTS as a narrow spectral peak on top of the broadband spectrum.

5.EDGE PLASMA STUDIES

Edge plasma analysis in stellarators is more complex than in tokamaks due to the inherent, strong non-axisymmetry. In addition, in the high ι range of W7-AS, island chains of symmetry n/m (with n=5 because of 5 field periods), are present at the boundary if the edge rotational transform ι_a = n/m. [1]. With the present target arrangement, the configuration is limiter-bounded at low ι (< 0.4), and separatrix-bounded at higher ι (>0.5). The edge plasma analysis has to consider increasing impacts of 3D effects with increasing edge collisionality. Consequently, the edge diagnostics is

designed to provide sufficiently three-dimensional parameter distributions. This is primarily achieved by a large number of Langmuir probes (radially movable, poloidal arrays and fast reciprocating, multi-tip probes). Additional diagnostics including the Li beam, μ-wave reflectometry, time of flight neutral analyzer (LENA), H_α arrays, spatially resolved spectroscopy and a video system were used for the characterization of the edge configuration and the transport. The experimental results can be related to edge plasma models (Sardei [14]).

In limiter ECRH plasmas at 2.5 T, relatively high edge temperatures were found ($\approx$ 50 to 100 eV). The magnitude and scaling of the transport in the SOL fits well to a continuation from inside the LCFS (Grigull et al. [15]).

The edge parameter phenomenology in island-bounded configurations was primarily studied in view of a planned installation of island divertor modules. The measurements were mainly focused on the questions how far the plasma parameter distributions reflect the vacuum field configurations (separatrix position, symmetry and size of islands, impact of finite plasma pressure), and to what extend the islands cause flux diversion. This was checked by 2D mapping of SOL n_e and T_e distributions. As an example, Fig. 12 shows n_e contours measured with the poloidal probe array at a fixed radial position for low β ECRH discharges versus the edge rotational transform ι_a. High densities (bright areas) indicate closed 5/m islands nearest to the respective probe tips. The contours demonstrate changes of the island symmetry from 5/11 to 5/8 with increasing ι_a. Values where the islands become intersected by the targets are indicated by sharp borders and doubling of the structures at the respective low ι_a sides (open-ended field lines inside the islands). Generally very good agreement with expectations from the vacuum field is found. There are clear indications for particle and energy flux diversion by the islands.

Based on these results a concept for an (open) island divertor was developed. Similar to the W7-X divertor concept (Kisslinger et al. [16]) the assembly will consist of ten identical modules placed close to the top and bottom of the elliptical plasma cross

sections of each magnetic field period (Fig. 13). The arrangement is completed by additional control loops (two per field period) for increased flexibility of the boundary configuration, and by Ti gettering systems for active pumping.

First code calculations obtained for the plasma parameters of a standard ECRH high density discharge predict peaked plasma densities inside the islands and at the toroidal location of the divertor plates. The recycling neutrals are ionized by more than 90 % outside the separatrix, the penetration of neutrals into the plasma core is reduced to an acceptable level.

7. CONCLUSIONS

A good diagnostic equipment is available in W7-AS for the characterization of 3-dimensional plasmas with a complex boundary structure. In the area of diagnostic development the potential of collective Thomson scattering (CTS) using a 140 GHz gyrotron was demonstrated in a proof of principle experiment for the first time. Extensive experimental investigations in different magnetic configurations were performed to verify their predicted properties with respect to equilibrium, stability and transport. In particular, the observed Shafranov shift is consistent with the expected reduction of the Pfirsch-Schlüter currents. The change of the rotational transform profile induced by these currents is still relatively large at high β and can cause low order rational surfaces to appear in the profile. This effect has been observed by pressure driven resonant MHD mode activity. The β-values, where the mode activity is correlated with degradation of the confinement, is in the proximity of the theshold given by the resistive interchange criterion. In the lower β range NBI driven GAE modes are detected, which are non-resonant ($\mathbf{k} \cdot \mathbf{B} \neq 0$) and formed and excited particularly in the presence of low shear.

Concerning neoclassical transport in the LMFP regime, some experimental evidence for effects due to the magnetic field ripple and the ambipolar electric field has been found.

The SOL is structured according to the vacuum field topology. In particular, evidence for boundary islands has been found, supporting the concept of an island divertor.

In stellarators, particular possibilities can be exploited for physics studies, such as investigations of and with local ECRH and ECCD.

References

[1] R. Jaenicke et al., High power heating experiments on WENDELSTEIN 7-AS stellarator, Invited papers from the 22nd EPS Conference on Controlled Fusion and Plasma Physics, Bournemouth, UK, 1995, to appear.

[2] J. Nührenberg, W. Lotz, P. Merkel, C. Nührenberg, U. Schwenn, E. Strumberger, T. Hayashi, Transactions of Fus. Techn. 27 (1995) 71.

[3] S.P. Hirshman et al., Comp. Phys. Comm. 43 (1986) 143

[4] A. Weller et al., Phys. Rev. Lett. 72 (1994) 1220.

[5] F. Wagner et al., Transactions of Fus. Techn. 27 (1995) 32.

[6] J.V. Hofmann et al., Proc. 21st EPS Conference on Controlled Fusion and Plasma Physics, Montpellier, 1994, Vol. 18B, Part I (1994) 372-375.

[7] WVII-A Team, NI Group, Nucl. Fusion 25 (1985)1593.

[8] R.Burhenn et al., Proc. of the 22nd EPS Conference on Controlled Fusion and Plasma Physics, Bournemouth,Vol. 19C, Part III (1995)145.

[9] E.Unger, PhD thesis, Max-Planck-Institut für Plasmaphysik, 1995, to appear.

[10] H.J. Hartfuss et al., Plasma Phys. Control. Fusion 36 (1994)B17.

[11] H.J. Hartfuss, V. Erckmann, A. Kechriniotis, W7-AS Team, to appear.

[12] V. Erckmann et al., Proc. of the 22nd EPS Conference on Controlled Fusion and Plasma Physics, Bournemouth,Vol. 19C, Part I (1995)357.

[13] E.V. Suvorov et al., Plasma Phys. and Contr. Fusion 37 (1995) 1207.

[14] F. Sardei et al., J. Nucl. Mater. 196-198 (1992)443.

[15] P. Grigull et al., Proc. of the Tenth Intern. Conf. on Stellarators, Madrid, EUR-CIEMAT 30 (1995)73.

[16] J. Kisslinger, C.D. Beidler, E. Harmeyer, F. Rau, H. Renner, H. Wobig, Proc. of the 22nd EPS Conference on Controlled Fusion and Plasma Physics, Bournemouth,Vol. 19C, Part III (1995)149.

Figure Captions

Fig. 1: Magnetic field coils and magnetic surfaces in W7-AS. Nonplanar modular coils (2 larger coils are seen) and additional planar toroidal coils.

Fig. 2: Magnetic field on axis (1 field period) for different configurations. The field ripple and field curvature can be varied by independent operation of the large modular coils or by a vertical field. The standard configuration correspond to the upper solid line.

Fig. 3: Observed β induced plasma shift derived from X-ray profiles (NBI heated shots in the low and high rotational transform regimes. The shift is clearly reduced with respect to predictions for the conventional $l = 2$ stellarator configuration (solid lines).

Fig. 4: High β equilibrium case ($< \beta > \approx 1.8\%$) calculated with NEMEC for an experimental case. The Shafranov shift seen in the upper part has caused a shift of the plasma axis by about 2/3 of the plasma radius, and leads to a strong modification of the iota profile with respect to the vacuum case (flat profile). The shaded area indicates a resistive interchange unstable region.

Fig. 5: Frequency spectrum of Mirnov signal. The peak around 20-30 kHz is due to Global Alfvén Eigenmodes (GAE), which are driven by fast NBI ions.

Fig. 6: Neoclassical ion and electron heat diffusivities as function of collisionality. In the LMFP regime ion coefficients are strongly reduced with increasing radial electric field (ambipolarity). In the left case, which corresponds to a transport reduced configuration (smaller ripple by inward shift), the heat diffusivities are reduced by a factor of ≈ 2 with respect to the standard configuration (right).

Fig. 7: Radial electric field from CXRS analysis (dots) and Langmuir probes (open circles) for an ECRH discharge at 2.5 T. The data are compared with a neoclassical calculation (solid line).

Fig. 8: X-ray signals from different radial channels showing the radial propagation of radiation from He- and H-like sulfur injected during gas-oscillation experiments. The source function is represented by the thick solid line (S II radiation observed by a grating spectrometer).

Fig. 9: The full width at half maximum (FWHM) of the Gauss fitted temperature modulation profiles as a function of modulation frequency for two different ECRH beamlines. Limiting values obtained by Lagrange extrapolation are given by the dotted lines labeled GyB and GyD.

Fig. 10: Phase profiles of the T_e-perturbation from ECE at two times. The heat wave is exited on plasma axis by ECRH power modulation. Perturbed regions are seen, which move radially inward.

Fig. 11: Thermal ion spectra in NBI sustained plasmas with $n_e = 0.35\ 10^{20}$ m^{-3} (experimental data: dots, theoretical fit curve: solid line). The fit gives $T_i = 480 \pm 80$ eV (440 ± 40 eV from CX).

Fig. 12: Contour plot of poloidal n_e distributions in the SOL (scale $3 \cdot 10^{17} \leq n_e \leq 1.5 \cdot 10^{18} m^{-3}$) measured by a poloidal Langmuir probe array versus ι_a. The pattern reflects the dominance of 5/m boundary islands.

Fig. 13: W7-AS island divertor at Φ=36° and 5/9 boundary islands.

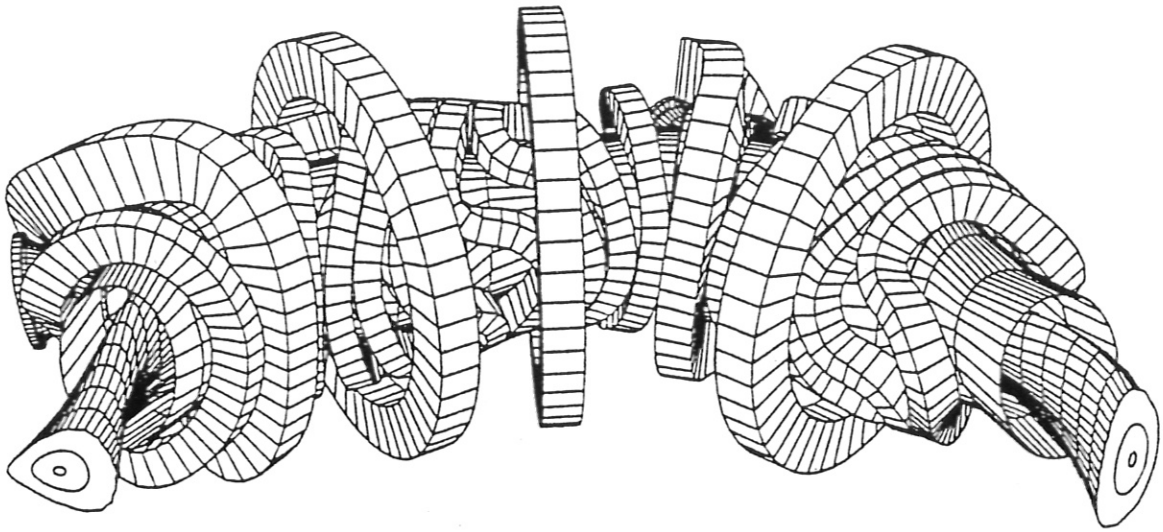

Fig. 1

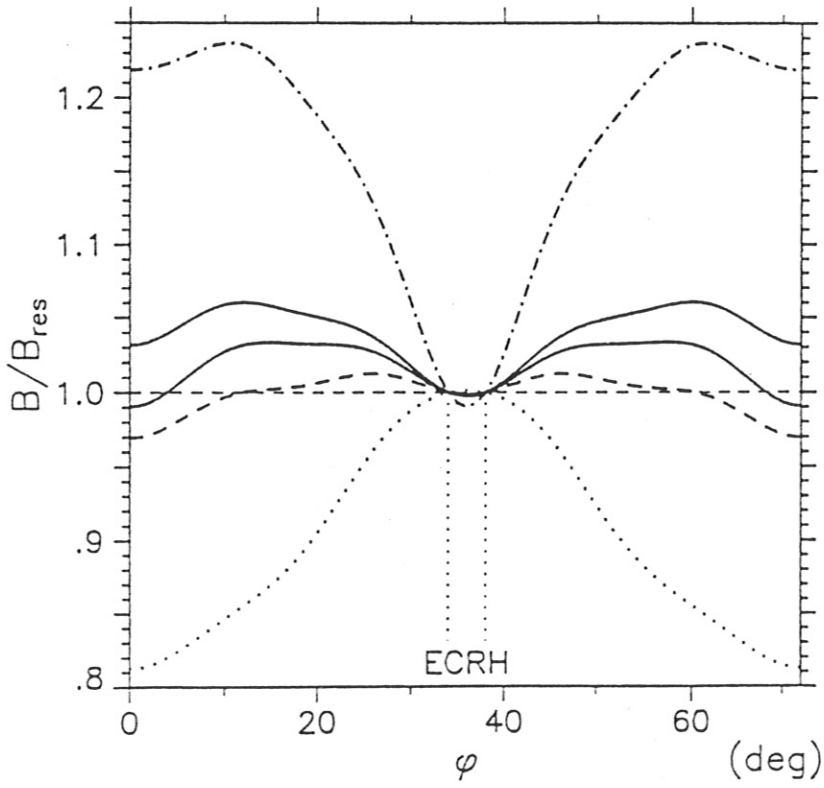

Fig. 2

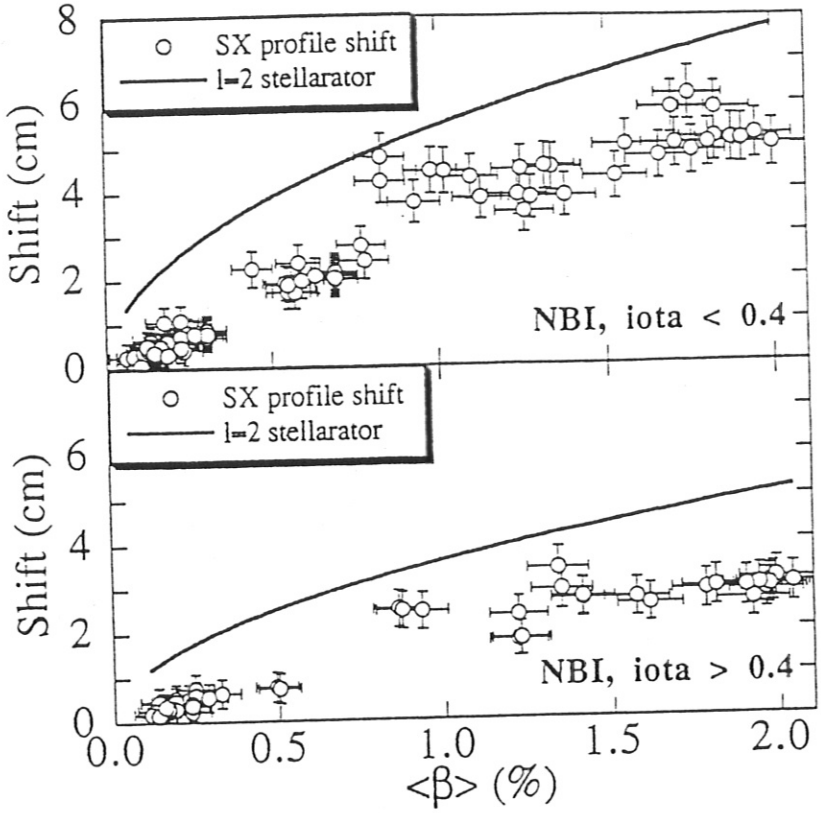
SX profile shift
l=2 stellarator
NBI, iota < 0.4
SX profile shift
l=2 stellarator
NBI, iota > 0.4
Shift (cm)
Shift (cm)
<β> (%)

Fig. 3

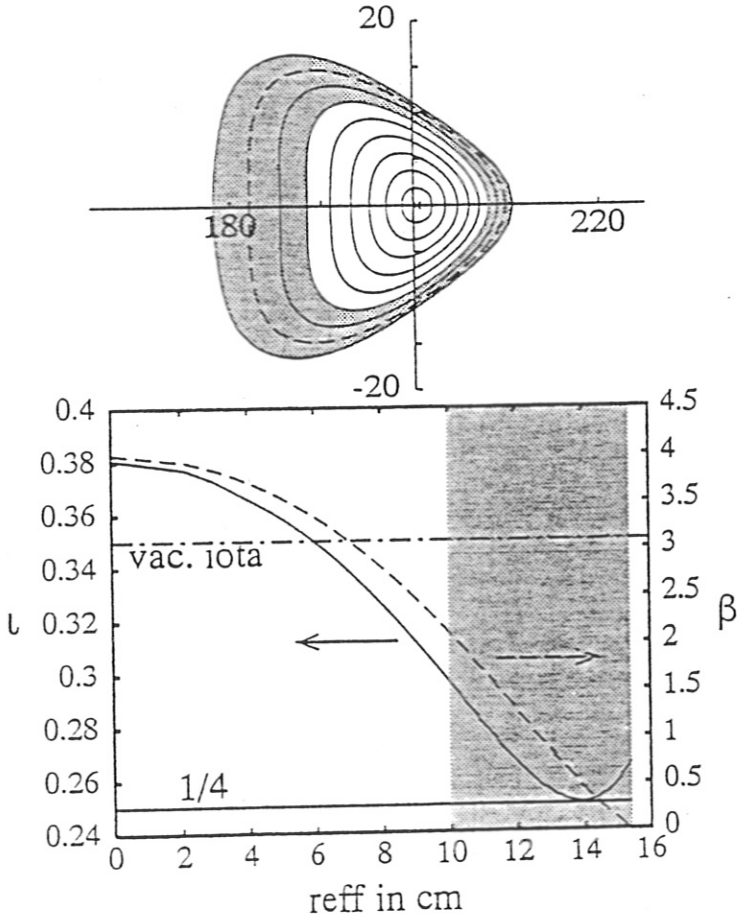
20
180
220
-20
vac. iota
1/4
ι
β
reff in cm

Fig. 4

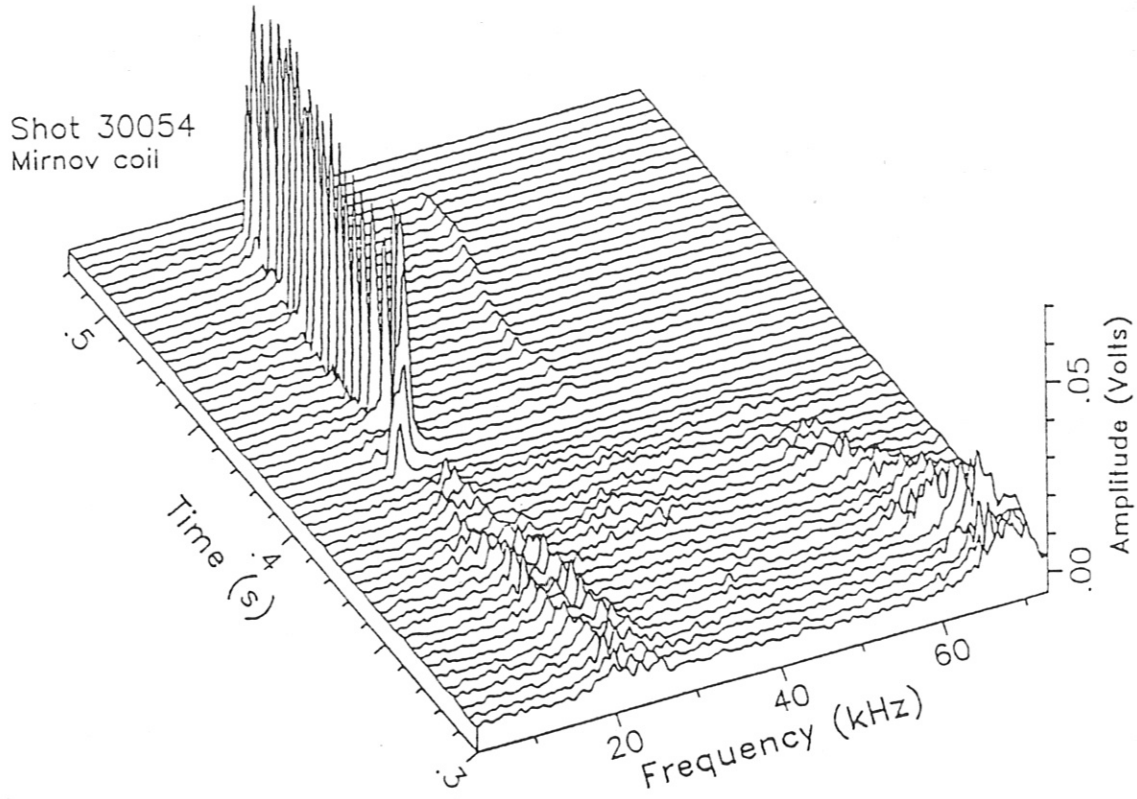
Shot 30054
Mirnov coil
.5
.4
.3
Time (s)
20
40
60
Frequency (kHz)
.00
.05
Amplitude (Volts)

Fig. 5

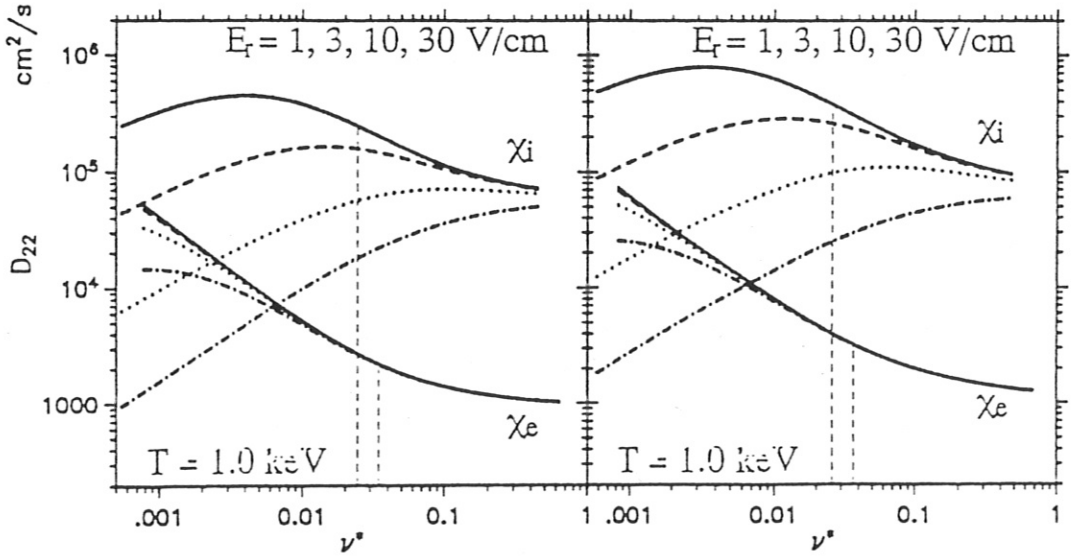
cm²/s
D22
10⁶
10⁵
10⁴
1000
Er = 1, 3, 10, 30 V/cm
χi
χe
T = 1.0 keV
.001
0.01
0.1
1
ν*
Er = 1, 3, 10, 30 V/cm
χi
χe
T = 1.0 keV
.001
0.01
0.1
1
ν*

Fig. 6

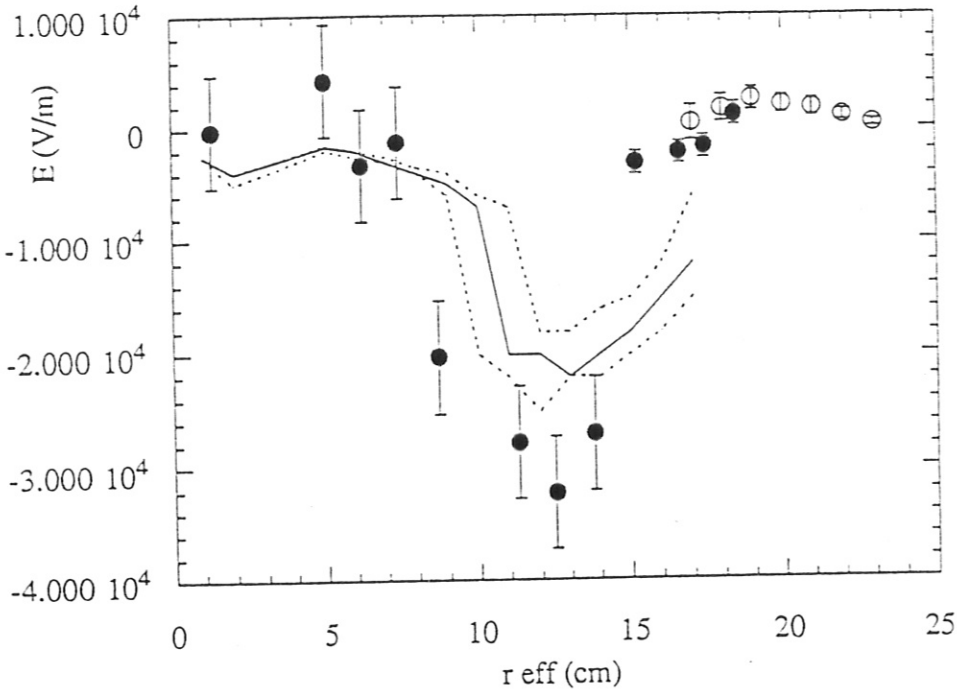
1.000 10^4
0
-1.000 10^4
-2.000 10^4
-3.000 10^4
-4.000 10^4
E (V/m)
0
5
10
15
20
25
r eff (cm)

Fig. 7

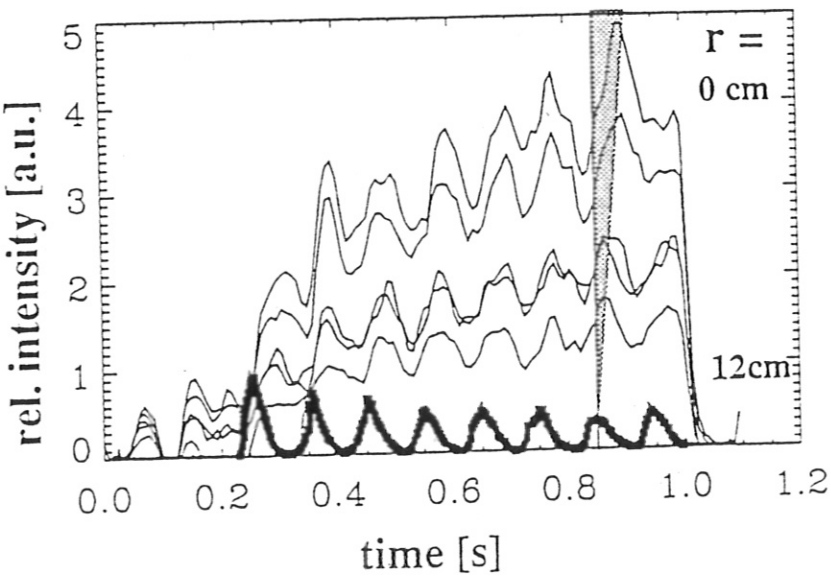
rel. intensity [a.u.]
0
1
2
3
4
5
0.0
0.2
0.4
0.6
0.8
1.0
1.2
time [s]
r =
0 cm
12cm

Fig. 8

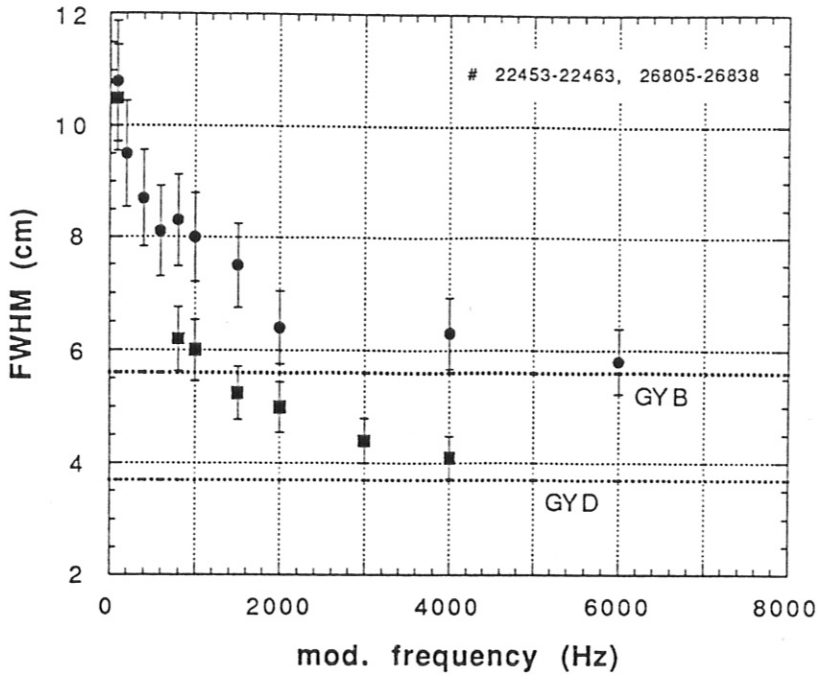
12
10
8
6
4
2
FWHM (cm)
22453-22463, 26805-26838
GYB
GYD
0
2000
4000
6000
8000
mod. frequency (Hz)

Fig. 9

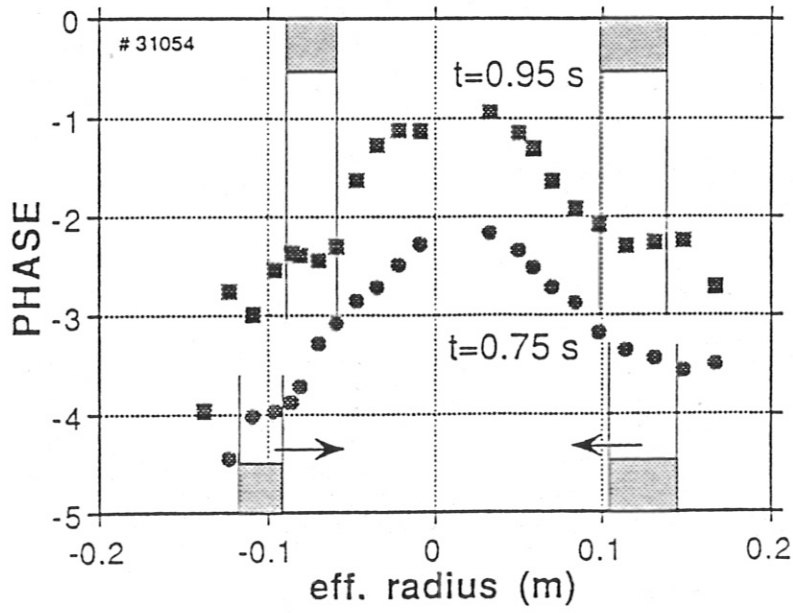
0
-1
-2
-3
-4
-5
PHASE
# 31054
t=0.95 s
t=0.75 s
-0.2
-0.1
0
0.1
0.2
eff. radius (m)

Fig. 10

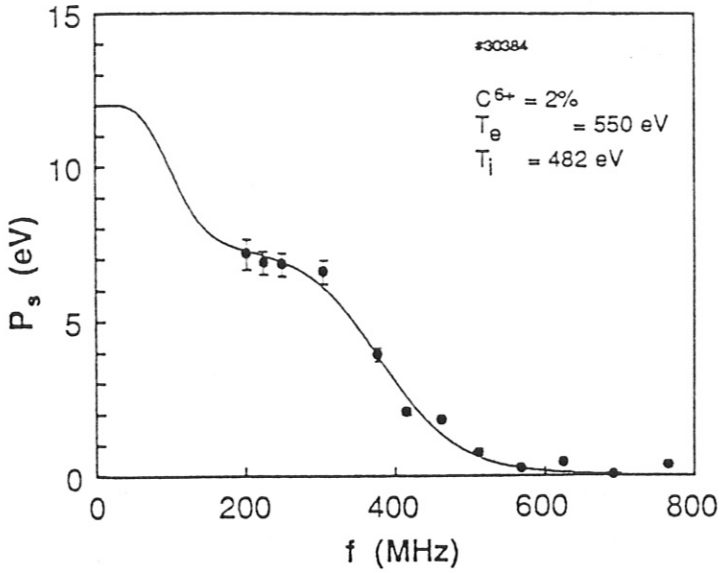
#30384
C6+ = 2%
Te = 550 eV
Ti = 482 eV
Ps (eV)
f (MHz)
0
5
10
15
0
200
400
600
800

Fig. 11

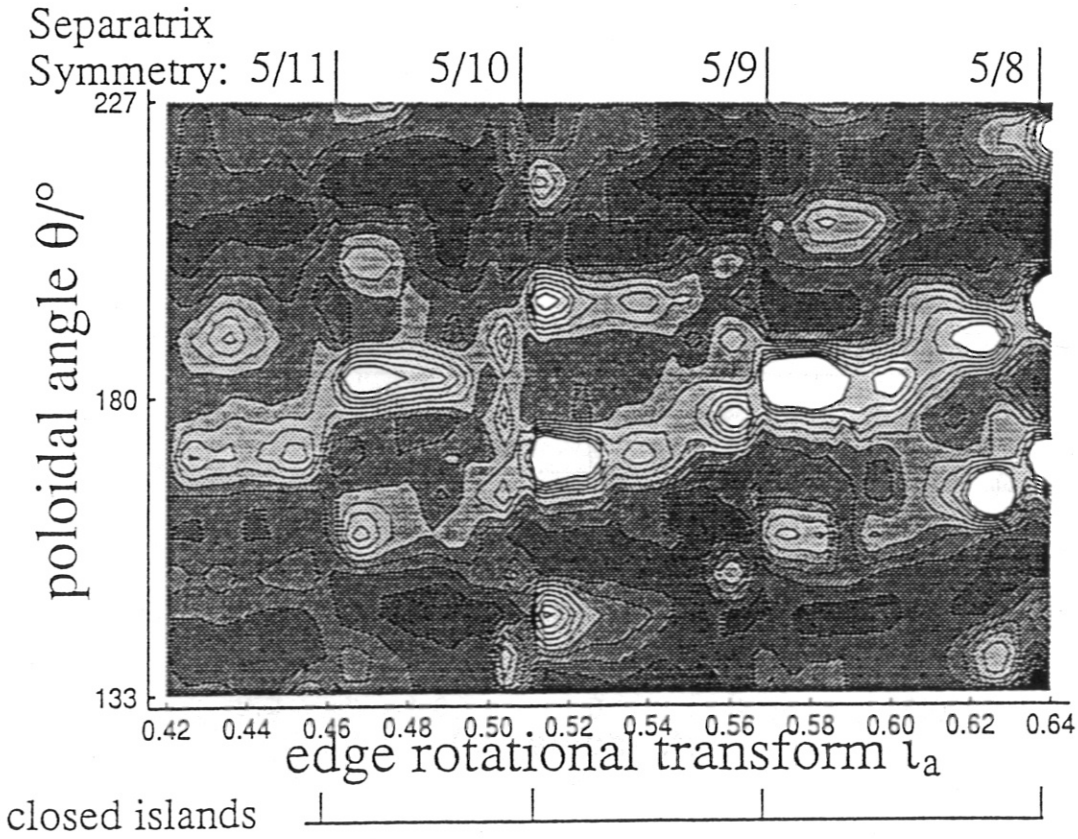
Separatrix
Symmetry: 5/11
5/10
5/9
5/8
poloidal angle θ/°
227
180
133
0.42
0.44
0.46
0.48
0.50
0.52
0.54
0.56
0.58
0.60
0.62
0.64
edge rotational transform ιa
closed islands

Fig. 12

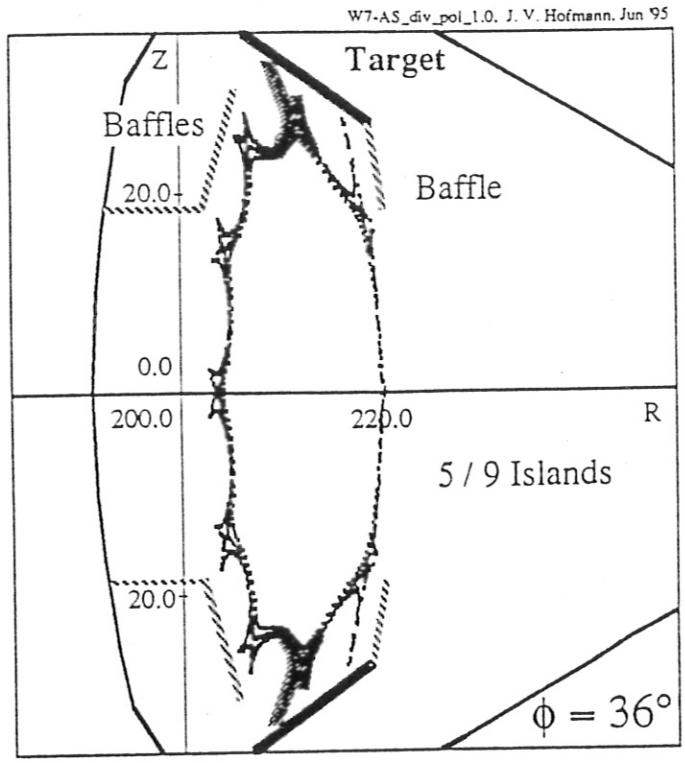
W7-AS_div_poi_1.0. J. V. Hofmann. Jun '95
Z
Target
Baffles
Baffle
20.0
0.0
200.0
220.0
R
5 / 9 Islands
20.0
ϕ = 36°

Fig. 13